NAVAL POSTGRADUATE SCHOOL
Monterey, California

THESIS

L6423

Investigation of a Heat Driven Thermoacoustic Prime Mover

by

Lin, Hsiao-Tseng

December 1989

Thesis Advisor: A. A. Atchley
Co-advisor T. J. Hofler

Approved for public release; distribution unlimited.

T247274

REPORT DOCUMENTATION PAGE

1a Report Security Classification: Unclassified	1b Restrictive Markings
2a Security Classification Authority	3 Distribution Availability of Report: Approved for public release; distribution is unlimited.
2b Declassification/Downgrading Schedule	
4 Performing Organization Report Number(s)	5 Monitoring Organization Report Number(s)
6a Name of Performing Organization: Naval Postgraduate School; 6b Office Symbol (*If Applicable*): 61	7a Name of Monitoring Organization: Naval Postgraduate School
6c Address (*city, state, and ZIP code*): Monterey, CA 93943-5000	7b Address (*city, state, and ZIP code*): Monterey, CA 93943-5000
8a Name of Funding/Sponsoring Organization; 8b Office Symbol (*If Applicable*)	9 Procurement Instrument Identification Number
8c Address (*city, state, and ZIP code*)	10 Source of Funding Numbers: Program Element Number; Project No; Task No; Work Unit Accession No

11 Title (*Include Security Classification*): INVESTIGATION OF A HEAT DRIVEN THERMOACOUSTIC PRIME MOVER

12 Personal Author(s): Lin, Hsiao-Tseng

13a Type of Report	13b Time Covered	14 Date of Report (*year, month,day*)	15 Page Count
Master's Thesis	From To	December 1989	75

16 Supplementary Notation: The views expressed in this thesis are those of the author and do not reflect the official policy or position of the Department of Defense or the U.S. Government.

17 Cosati Codes			18 Subject Terms (*continue on reverse if necessary and identify by block number*)
Field	Group	Subgroup	Acoustics, Thermoacoustics, Thermoacoustic Heat Transport

19 Abstract (*continue on reverse if necessary and identify by block number*)

The goal of this thesis is to investigate the work output of a heat driven thermoacoustic prime mover. The experimental approach was to measure the frequency response of both a simple resonant tube and a prime mover for a variety of values of mean gas pressure and applied temperature difference across the prime mover stack. A least squares fit to the frequency response yields the quality factor which can be compared to predictions based on a short stack, boundary layer approximation theory by Swift [J. Acoust. Soc. Am. 84, 1145-1180 (1988)]. The results are reported of measurements made on the lowest three modes of the prime mover in helium for mean gas pressures between approximately 170 kPa and 500 kPa and the applied temperature differences between zero and onset. The signal waveforms of the sound generated by the prime mover above onset at a mean gas pressure of 308 kPa are also reported. Results for the resonant tube have at most 3% difference with theory. For the prime mover, the measurements generally agree with predictions for the fundamental mode except close to onset. This agreement between measured and predicted results worsens with decreasing mean gas pressure. Agreement is poor for the second and third modes for all pressures used. Finally, the sound generated by the prime mover above onset is highly distorted, and the distortion becomes more serve as the temperature difference increases. The peak positive pressure amplitude of this signal at temperature difference of 325 °C, 368 °C and 453 °C are 1.1%, 4.4% and 7.9% of mean gas pressure, respectively.

20 Distribution/Availability of Abstract	21 Abstract Security Classification	
[X] unclassified/unlimited [ ] same as report [ ] DTIC users	Unclassified	
22a Name of Responsible Individual: Anthony A. Atchley	22b Telephone (*Include Area code*): (408) 646-2848	22c Office Symbol: 61Ay

Approved for public release; distribution is unlimited.

Investigation of a Heat Driven Thermoacoustic Prime Mover

by

Lin, Hsiao-Tseng
Captain, Taiwan Army
B.S., Chung Cheng Institute of Technology in Taiwan, 1984

Submitted in partial fulfillment of the requirements
for the degree of

MASTER OF SCIENCE IN ENGINEERING ACOUSTICS

from the

NAVAL POSTGRADUATE SCHOOL
December 1989

ABSTRACT

The goal of this thesis is to investigate the work output of a heat driven thermoacoustic prime mover. The experimental approach was to measure the frequency response of both a simple resonant tube and a prime mover for a variety of values of mean gas pressure and applied temperature difference across the prime mover stack. A least squares fit to the frequency response yields the quality factor which can be compared to predictions based on a short stack, boundary layer approximation theory by Swift [J. Acoust. Soc. Am. 84, 1145-1180 (1988)]. The results are reported of measurements made on the lowest three modes of the prime mover in helium for mean gas pressures between approximately 170 kPa and 500 kPa and the applied temperature differences between zero and onset. The signal waveforms of the sound generated by the prime mover above onset at a mean gas pressure of 308 kPa are also reported. Results for the resonant tube have at most 3% difference with theory. For the prime mover, the measurements generally agree with predictions for the fundamental mode except close to onset. This agreement between measured and predicted results worsens with decreasing mean gas pressure. Agreement is poor for the second and third modes for all pressures used. Finally, the sound generated by the prime mover above onset is highly distorted, and the distortion becomes more serve as the temperature difference increases. The peak positive pressure amplitude of this signal at temperature difference of 325 °C, 368 °C and 453 °C are 1.1%, 4.4% and 7.9% of mean gas pressure, respectively.

Th513
L64/012
c.1

TABLE OF CONTENTS

LIST OF SYMBOLS

c	sound speed
c_P	isobaric heat capacity per unit mass
$\dot{E}$	dissipated acoustic power
$\dot{e}$	dissipated acoustic power per unit area
f	frequency
f_o	measured resonance frequency
$\mathbf{k}$	complex wave number, $\mathbf{k} = k - i\,\alpha$
L	resonator length
l	plate half-thickness
P_A	peak acoustic pressure amplitude
$\mathbf{p}$	complex acoustic pressure
Q	quality factor
Re	real part of
S	cross section area
S_D	surface area of driver
T	temperature
U_D	volume velocity of driver
V_D	volume displaced by driver
$\dot{W}$	generated acoustic power
x	position along tube axis

LIST OF SYMBOLS (CONTINUED)

y_o plate half-gap

$\mathbf{Z}_{mo}$ complex mechanical impedance, $\mathbf{Z}_{mo} = R_{mo} + i\, Z_{mo}$

α absorption coefficient

β thermal expansion coefficient

Δx plate length

δ_s thermal penetration depth in the solid plate

δ_κ thermal penetration depth in the gas

δ_υ viscous penetration depth in the gas

ε_s plate heat capacity ratio

Γ normalized temperature gradient

γ ratio of isobaric to isochoric specific heats

Π perimeter

ρ_m mean gas density

ρ_s density of solid

σ Prandtl number

ξ_D displacement of driver

ACKNOWLEDGMENTS

First and foremost, I would like to thank the Lord who allowed me to learn so much, not just about acoustics, but more importantly, about how to believe and count on Him.

I want to express my sincere appreciation to my advisors, Dr. Anthony Atchley and Dr. Thomas Hofler for their encouragement, words of wisdom and infinite patience.

Next I thank George Jaksha and Steven Blankschein of the physics machine shop for their help in conducting my experiment. I also thank my classmate David Pierce and my sponsor Michael Weisskopf who spent a great deal of time to help me in writing and typing skills.

Finally, I reserve special thanks for the support from my family, even though they are far away overseas.

May the Lord bless them all.

I. INTRODUCTION

There are two basic classes of thermoacoustic engines: heat pumps and prime movers [Refs. 1-3]. A thermoacoustic heat pump uses a high amplitude acoustic standing wave to transport (or pump) heat along, for example, the boundary of a plate situated in the standing wave. This acoustically generated heat flow results in a thermal gradient being established across the plate. In other words, acoustic energy is converted into stored thermal energy, which in turn can be used in a number of practical applications. Thermoacoustic prime movers, on the other hand, convert stored thermal energy into useful work in the form of sound. Such a device is the subject of this thesis.

Referring to Figure 1, a typical prime mover configuration consists of a stack of plates, called the prime mover stack (or, simply, the stack), which is in thermal contact with two heat exchangers. In this thesis, the two heat exchangers will be called the hot and ambient heat exchangers, because one end of the prime mover stack will be held at elevated temperatures while the other end will be held at ambient (room) temperature. However, the important quantity is the temperature difference across the prime mover stack, not the absolute temperatures of either end. Hence, if (what we called) the hot end were to be held at ambient temperature, and (what we called) the ambient end held at temperatures below ambient, the process described in this thesis would fundamentally be the same. An example of an ambient/cold prime mover is the, so called, "Hofler tube", described elsewhere [Refs. 3-4]. As also indicated in Figure 1, the prime mover stack and heat exchangers are housed within an

acoustic resonator. The prime mover stack/heat exchanger/resonator assembly is called a (thermoacoustic) prime mover.

Thermal energy is stored in the prime mover by imposing a temperature difference across the stack, the two quantities being proportional. In order for the prime mover to produce net positive work, i.e. to produce audible sound, the amount of stored energy converted to sound must exceed the amount of acoustic energy dissipated by losses in the prime mover. The dominant loss mechanism for the type of gases and frequencies of interest here are thermal and viscous losses at the resonator walls and the stack and heat exchanger surfaces. The prime mover is said to have reached "onset" when the temperature difference across the stack is sufficient for the prime mover to generate and sustain detectable levels of sound. The use of the word "detectable" is not meant to imply that onset is a subtle question of detection thresholds. Our experience is that when onset is reached, the observer (and everyone else in the room) knows it.

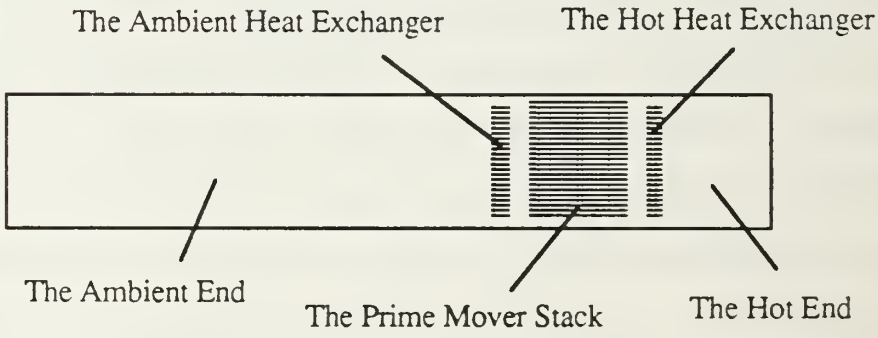

Figure 1 - A typical prime mover configuration

The investigation of a prime mover is conveniently divided into two parts: below and above onset. The main goal of this paper is to investigate the approach to onset of a thermoacoustic prime mover. However, brief mention will be made of the behavior above onset. As will be discussed, there are a number of added complications above onset.

In order to investigate the work output of a prime mover, use will be made of the fact that the temperature difference across the stack affects the net absorption in the prime mover. As the temperature difference increases from zero to its value at onset, the net absorption decreases to zero. The absorption coefficient can be determined by measuring the quality factor Q of the prime mover, which, in turn, can be related to the acoustic power dissipated in the tube. The power can be calculated using equations derived by Swift [Ref. 1], which express the acoustic power output of a thermoacoustic engine as a function of the applied temperature difference across the stack.

Swift presents a detailed theoretical development in his review article. However, as he shows, the theory results in relatively simple expressions if the short stack and boundary layer approximation are made. The theoretical predictions presented in this thesis are based on this approximate theory, in order to test the ranges of its validity.

II. THEORY

The measurements performed in the prime mover yield its Q as a function of the applied temperature difference. However, the quantity most conveniently computed from theory is the net acoustic power dissipated by the prime mover. The relationship between these two quantities is derived in this chapter.

The dependence of the acoustic pressure with distance for a plane wave in a closed, rigid, cylindrical tube of length L and cross section area S is given by [Ref. 5 Equation (9.26)]

$$\mathbf{p}(x,t) = P_A \frac{\cos[\mathbf{k}(L-x)]}{\cos \mathbf{k}L} e^{i\omega t}, \tag{1}$$

where $\mathbf{k} = k - i\alpha$. The input mechanical impedance presented to a driver located at $x = 0$ is therefore given by

$$\mathbf{Z}_{mo} = -i\rho_m \frac{\omega}{\mathbf{k}} S \cot \mathbf{k}L . \tag{2}$$

In steady state, the power dissipated by the tube is equal to that delivered by the driver, which is given by

$$\dot{E} = \frac{P_A^2 S^2 R_{mo}}{2 Z_{mo}^2}, \tag{3}$$

where $R_{mo} = Re\{\mathbf{Z}_{mo}\}$ and $Z_{mo} = |\mathbf{Z}_{mo}|$. Under conditions of resonance for a rigid tube, sin kL = 0, Equation 3 reduces to

$$\dot{E} = \frac{1}{2}\frac{P_A^2}{\rho_m c} S\alpha L . \tag{4}$$

The absorption coefficient α can be related to the quality factor Q_n of the n^{th} mode of the tube by $\alpha = \omega_n/2Q_n c$. (The subscript n will be dropped unless there is potential for confusion). Substituting this relationship into Equation 4 and solving for 1/Q gives

$$\frac{1}{Q} = \frac{4\rho_m c^2}{P_A^2 \omega LS}\dot{E} . \tag{5}$$

As indicated in Figure 1, a prime mover is comprised of five parts: the hot end, the hot heat exchanger, the prime mover stack, the ambient heat exchanger, and the ambient end. Accordingly, the power dissipated by the prime mover can be separated into five parts as

$$\dot{E} = \dot{E}_{\substack{amb \\ end}} + \dot{E}_{\substack{amb \\ htex}} + \dot{E}_{stack} + \dot{E}_{\substack{hot \\ htex}} + \dot{E}_{\substack{hot \\ end}} , \tag{6}$$

where the five terms represent the power dissipated by the ambient end, the ambient heat exchanger, the prime mover stack, the hot heat exchanger, and the hot end, respectively.

Using results from Swift's review article [Ref. 1], expressions can be found for the five terms on the right-hand side of Equation 6. We begin with Swift's expression for the acoustic power generated by a short thermoacoustic engine [Ref. 1 Equation 80]

$$\dot{W} = \frac{1}{4}\Pi\delta_\kappa \Delta x \omega \cos^2(kx)\frac{P_A^{\,2}}{\rho_m c^2} \times \left[\frac{(\gamma-1)}{(1+\varepsilon_s)}\left(\frac{\Gamma}{\left(1+\sqrt{\sigma}\right)\left(1-\delta_v/y_o+\delta_v^2/2y_o^2\right)}-1\right)-\frac{\delta_v}{\delta_\kappa}\frac{\left(1+l/y_o\right)^2}{\left(1-\delta_v/y_o+\delta_v^2/2y_o^2\right)}\tan^2(kx)\right], \tag{7}$$

where $\varepsilon_s = \rho_m\, c_p\, \delta_\kappa / \rho_s\, c_p\, \delta_s$, $\Gamma = \nabla T / \nabla T_{crit}$, $\nabla T = \Delta T / \Delta x = (T_{hot} - T_{amb})/\Delta x$, and

$$\nabla T_{crit} = \frac{T\beta}{c_p}\omega c \frac{\cot kx}{1+l/y_o}. \tag{8}$$

It is assumed in deriving this expression that the stack is short compared to the radian wavelength ($\Delta x << \lambda/2\pi$), the boundary layer approximation ($y_o >> \delta_v$, $y_o >> \delta_\kappa$ and $l >> \delta_s$) is valid and that $\Delta T << T$. It should be pointed out that this equation differs from Swift's in that we assume the pressure to vary as cos(kx), rather than sin(kx).

Two modifications, involving conventions, must be made to Equation 7 before it can be applied to our problem. $\dot{W}$ in Equation 7 is positive when power

is generated. However, the convention in Equation 5 is that $\dot{E}$ is positive when power is dissipated. Hence, $\dot{E} = -\dot{W}$. Finally, the sign convention of ΔT must be reversed relative to Swift's convention because we will measure x from the ambient end, whereas Swift measures x from the hot end. In order to accommodate this change, a minus sign will be introduced in front of Γ. With these conventions in mind, we arrive at an expression for the acoustic power dissipated by a short thermoacoustic engine

$$\dot{E} = \frac{1}{4}\Pi\delta_\kappa \Delta x \omega \frac{P_A^2}{\rho_m c^2}\cos^2(kx) \times \left[\frac{(\gamma-1)}{(1+\varepsilon_s)}\left(1+\frac{\Gamma}{\left(1+\sqrt{\sigma}\right)\left(1-\delta_\nu/y_o+\delta_\nu^2/2y_o^2\right)}\right)+\frac{\delta_\nu}{\delta_\kappa}\frac{\left(1+l/y_o\right)^2}{\left(1-\delta_\nu/y_o+\delta_\nu^2/2y_o^2\right)}\tan^2(kx)\right]. \quad (9)$$

Again following Swift, the contribution to Equation 6 from the ambient and hot ends of the resonator can be found by realizing that the power dissipated per unit area $\dot{e}$ of the resonator can be found by dividing Equation 9 by the surface area of the engine $\Pi\Delta x$, setting $\Gamma = 0$, $l = 0$, and assuming that $\delta_\nu << y_o$. The justification for letting $\Gamma = 0$ is that the temperature is uniform throughout these parts of the prime mover. The justification for setting $l = 0$ is that the $(1 + l/y_o)$ term accounts for the increase in volume velocity upon entering the stack. If there is no stack then this term in unnecessary. Finally, the tube radius R assumes the role of y_o in the absence of the stack. For the frequencies, gases, mean pressures, and tube radius of interest, δ_ν/R in on the order of 10^{-2} to 10^{-3}.

These modifications to Equation 9 yield, for the power dissipated per unit area of the resonator

$$\dot{e} = \frac{1}{4}\delta_\kappa \omega \frac{P_A^2}{\rho_m c^2}\cos^2(kx)\left[\frac{(\gamma-1)}{(1+\varepsilon_s)} + \frac{\delta_\nu}{\delta_\kappa}\left(1 + l/y_o\right)^2 \tan^2(kx)\right]. \tag{10}$$

Integration of this expression over the surface area of the ambient and hot ends of the resonator yields expressions for $\dot{E}_{end}^{amb}$ and $\dot{E}_{end}^{hot}$

$$\dot{E}_{end}^{amb} = \frac{P_A{}^2 \omega L S \delta_\kappa}{4\rho_m c^2 R}\frac{(\gamma-1)}{(1+\varepsilon_s)}\left[\frac{x_{amb}}{L} + \frac{\sin(2kx_{amb})}{kL}\right] + \frac{P_A{}^2 \omega L S \delta_\nu}{4\rho_m c^2 R}\left[\frac{x_{amb}}{L} - \frac{\sin(2kx_{amb})}{kL}\right] + \frac{\delta_\kappa}{L}\frac{(\gamma-1)}{(1+\varepsilon_s)} \tag{11}$$

and

$$\dot{E}_{end}^{hot} = \frac{P_A{}^2 \omega L S \delta_\kappa}{4\rho_m c^2 R}\frac{(\gamma-1)}{(1+\varepsilon_s)}\left[\frac{L-x_{hot}}{L} - \frac{\sin(2kx_{hot})}{kL}\right] + \frac{P_A{}^2 \omega L S \delta_\nu}{4\rho_m c^2 R}\left[\frac{L-x_{hot}}{L} + \frac{\sin(2kx_{hot})}{kL}\right] + \frac{\delta_\kappa}{L}\frac{(\gamma-1)}{(1+\varepsilon_s)}. \tag{12}$$

The thermophysical properties are to be evaluated for either the ambient or hot end, depending on which term is to be computed.

The contributions to Equation 6 from the ambient and hot heat exchangers is found by setting $\Gamma = 0$ in Equation 9 (because the temperature is assumed to be

uniform across the heat exchangers) and substituting the result into Equation 5. The result is

$$\dot{E}_{\substack{amb/hot \\ ht\,ex}} = \frac{P_A^2 \omega \Pi \delta_\kappa \Delta x}{4\rho_m c^2} \cos^2(kx) \left[\frac{(\gamma - 1)}{(1 + \varepsilon_s)} + \frac{\delta_\nu}{\delta_\kappa} \frac{(1 + l/y_o)^2}{\left(1 - \delta_\nu/y_o + \delta_\nu^2/2y_o^2\right)} \tan^2(kx) \right], \quad (13)$$

where the geometrical properties of the exchangers and the thermophysical properties are to be evaluated for either the ambient or hot heat exchangers, depending on which terms are to be computed.

The stack's contribution to Equation 6 is found by substituting Equation 9 directly into Equation 5 to give

$$\dot{E}_{stack} = \frac{P_A^2 \omega \Pi \delta_\kappa \Delta x}{4\rho_m c^2} \cos^2(kx) \quad (14)$$

$$\times \left[\frac{(\gamma - 1)}{(1 + \varepsilon_s)} \left(\frac{\Gamma}{\left(1 + \sqrt{\sigma}\right)\left(1 - \delta_\nu/y_o + \delta_\nu^2/2y_o^2\right)} + 1 \right) + \frac{\delta_\nu}{\delta_\kappa} \frac{(1 + l/y_o)^2}{\left(1 - \delta_\nu/y_o + \delta_\nu^2/2y_o^2\right)} \tan^2(kx) \right].$$

Because, as discussed later the initial phases of this experiment consist of measuring the Q of an empty, rigidly terminated, cylindrical resonator, we give an expression for the Q of such a system. The losses in the empty resonator can be found by integrating Equation 10 over the surface area of the entire resonator. Substitution of the result into Equation 5 yields

$$\frac{1}{Q_{\substack{\text{empty}\\\text{tube}}}} = \frac{\delta_\kappa}{R}\frac{(\gamma-1)}{(1+\varepsilon_s)} + \frac{\delta_\nu}{R} + \frac{2\,\delta_\kappa}{L}\frac{(\gamma-1)}{(1+\varepsilon_s)}, \tag{15}$$

where is identical to Swift's result [Ref. 1 Equation 91].

In order to obtain the Q of the prime mover, it will be driven at frequencies in the neighborhood of a resonance with a high impedance source and measure the amplitude of the output of a high impedance receiver. Both the source and receiver are located at the rigid end of the ambient section of the prime mover, i.e. at x = 0. The fitting function is found by considering the acoustic impedance seen by the driver. The driver used in these measurements is an electret transducer, which acts as a constant displacement source, if the driving voltage is constant. The volume velocity of the driver U_D is given by

$$U_D = \xi_D S_D \omega = V_D \omega, \tag{16}$$

where ξ_D and S_D are the displacement and surface area of the driver, respectively. V_D is, therefore, the volume displaced by the driver. The pressure is equal to the product of the acoustic impedance **Z** and the volume velocity. The acoustic impedance is related to the mechanical impedance by $\mathbf{Z} = \mathbf{Z}_m/S^2$. Therefore, the complex pressure amplitude at x = 0 is given by

$$\mathbf{p}(0) = \frac{\rho_m V_D}{S}\frac{\omega^2}{\mathbf{k}}\cot \mathbf{k}L, \tag{17}$$

where use has been made of Equation 2.

The magnitude of the pressure at x = 0 is thus

$$p = |\mathbf{p}(0)| = \frac{\rho_m L V_D}{S}\omega^2 \left| \frac{\cot \mathbf{kL}}{\mathbf{kL}} \right|. \tag{18}$$

Using the relation k= ω/c, $k_oL = \pi$ and $Q=\omega_o/2\alpha c$, the factor **kL** can be related to ω_o and Q by

$$\mathbf{kL} = \pi\left(\frac{\omega}{\omega_o} - \frac{i}{2Q}\right). \tag{19}$$

By further defining $A = \rho_m V_D L \omega_o^2 / S$, Equation 19 can be expressed in terms of the three parameters A, Q, and ω_o as

$$p = A\left(\frac{\omega}{\omega_o}\right)^2 \left| \frac{\cot\left[\pi\left(\frac{\omega}{\omega_o} - \frac{i}{2Q}\right)\right]}{\pi\left(\frac{\omega}{\omega_o} - \frac{i}{2Q}\right)} \right|. \tag{20}$$

A three parameter, least squares fit of this function to the measured data is used to obtain Q and ω_o for the analysis discussed below.

The question may arise as to the validity of using the assumptions associated with Equation 1, in particular, that the losses, represented by the imaginary part of the complex propagation constant ($\mathbf{k} = k - i\alpha$), are distributed uniformly along the length of the tube. Such is certainly not the case in the prime mover. The answer lies in the fact that the quantity of interest is the frequency response

of the prime mover, not the variation of the acoustic pressure with distance, or even the absolute acoustic pressure in the prime mover. Over a small band of frequencies, the pressure amplitude at a particular point should depend only on the total attenuation in the tube, not on its spatial distribution. When use is made of the relation $\alpha = \omega/2Qc$, α represents the effective absorption coefficient due to uniformly distributed losses that would give the same Q as the one actually measured. As long as we limit ourselves to finding the frequency response, the formalism associated with Equation 1 is valid.

III. EXPERIMENT APPARATUS AND PROCEDURE

The primary goals are to measure the quality factor of the heat driven prime mover below onset as a function of the mean gas pressure and the applied temperature difference, and the waveform of the sound generated above onset. In order to gain confidence in our ability to measure the quality factor, we measured the Q of a simple configuration called the resonant tube, shown in Figure 2. This resonant tube was then modified by adding the ambient heat exchanger and changing the upper portion to one consisting of the prime mover stack and the hot heat exchanger. This configuration (Figure 3) is called the heat driven prime mover. A final configuration was built to observe the behavior above onset. This configuration is virtually identical to the heat driven prime mover, except that the electret driver is replaced by a high intensity pressure transducer. This chapter is divided into four sections as follows: (A) The resonant tube. (B) The heat driven prime mover. (C) Temperature control equipment. (D) Instrumentation and procedure.

A. THE RESONANT TUBE

1. The Tube

The tube is made from two 3.82 cm ID copper tubes, separated by a brass ambient heat exchanger container. The two sections of copper tube are 11.4 cm and 88.1 cm long. The other end of the two sections are fitted with flanges which allow them to be soldered to the ambient heat exchanger container. The total length of the resonator, including the heat exchanger container, is

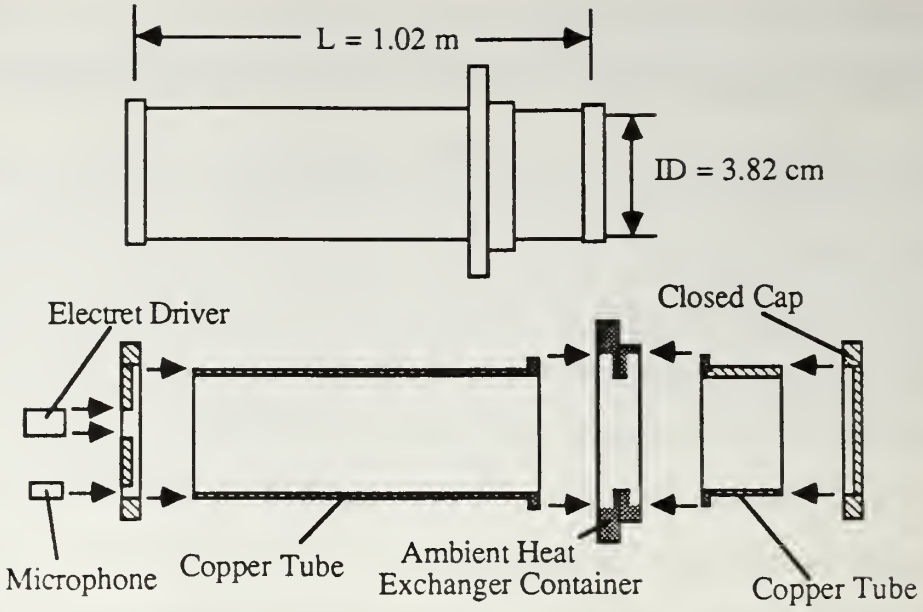

Figure 2 - The resonant tube configuration

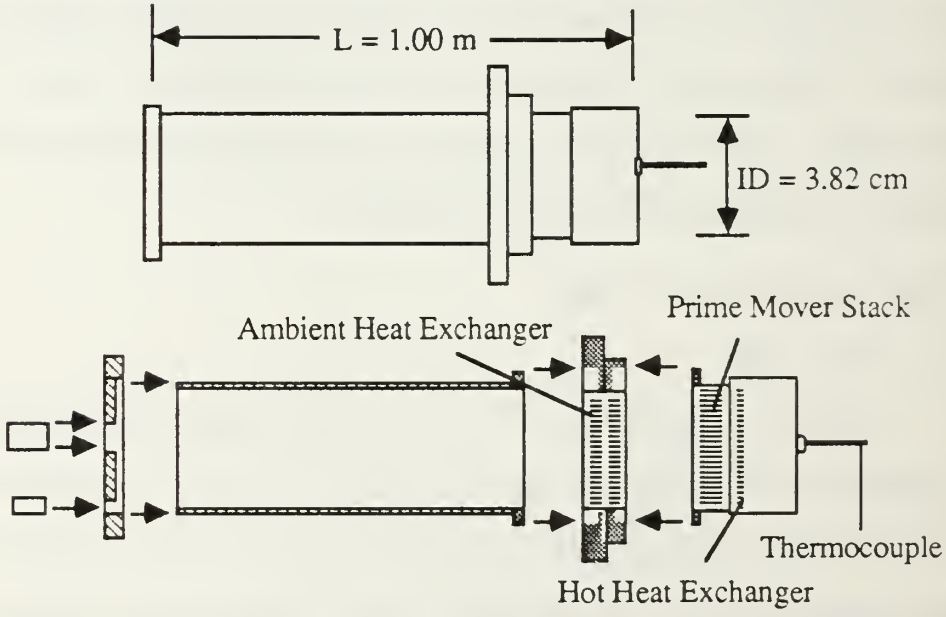

Figure 3 - The Heat Driven Prime Mover

1.02m (internal dimensions). A copper cap is soldered to the end of the shorter section, forming a closed, rigid, termination. There is also a copper end cap for the longer section. However, this cap houses an electret driver and a tiny electret microphone. The driver and microphone are flush mounted and sealed in the end cap with epoxy. The end cap is epoxied to the section of tube. The resonator is connected to a gas handling system, through a valve in the ambient heat exchanger container, to allow pressurization with helium. A vacuum pump evacuated the resonator before filling with helium. A system vent is also provided. In order to sense the mean pressure inside the tube, a dial pressure gauge and an OMEGA Model PX304-150AV pressure transducer are connected to the fill line.

2. Driver and Microphone

It is desired that the impedance of the end cap containing the driver and microphone be large compared to the highest acoustic impedance of the standing wave. This requirement can be accomplished by using electret designs. An 1.9 cm electret transducer was constructed for use as the acoustic driver. The input signal is provided by a Hewlett Packard Model 8904A Multifunction Synthesizer and amplified by a Techron Model 7520 power amplifier. A tiny, 0.594 cm diameter, Panasonic electret microphone was used to sense the response. The output signal is amplified by a signal amplifier with an open loop gain of 100.

B. THE HEAT DRIVEN PRIME MOVER

As explained in the previous chapter, the heat driven prime mover consists of hot and ambient heat exchangers and a prime mover stack. These devices are described in this section.

1. The Heater Section and Hot Heat Exchanger

The purpose of the hot heat exchanger is to supply heat to the prime mover stack. As shown in Figure 4, the hot end of the prime mover consists of a nickel heater section and a heat exchanger. The heater section consists of a 3.82 cm ID, 5.00 cm long, nickel tube. One end of the tube is capped and drilled to accommodate a thermocouple probe, used to sense the hot heat exchanger temperature. The other end of the heater section contains the heat exchanger consisting of 25, 0.051 cm thick, 0.762 cm long nickel plates. The gap between each pair of adjacent plates is 0.102 cm. Between each plates there is a 304 stainless steel spacers with a length of 0.102 cm and a diameter of 0.031 cm.

2. The Ambient Heat Exchanger

In order to impose a temperature gradient across the prime mover stack, an ambient heat exchanger is employed to maintain one end of the stack at a constant ambient temperature. The construction of this heat exchanger is very similar to the hot heat exchanger, except it has a length of 1.02 cm and contains 25 copper plates. The ambient heat exchanger actually consists of two such stacks separated by a 0.15 cm gap as shown in Figure 5.

3. The Prime Mover Stack

This stack is the heart of the heat driven prime mover. A temperature gradient will be established across this stack to supply the required heat flux. As shown in Figure 6, the prime mover stack consists of a cylindrical stainless steel shell containing 35, 0.25 cm thick 304 stainless steel plates 3.42 cm long spaced by 0.079 cm .

A complete listing of the specifications of the heat exchangers and the prime mover stack is provided in Appendix C.

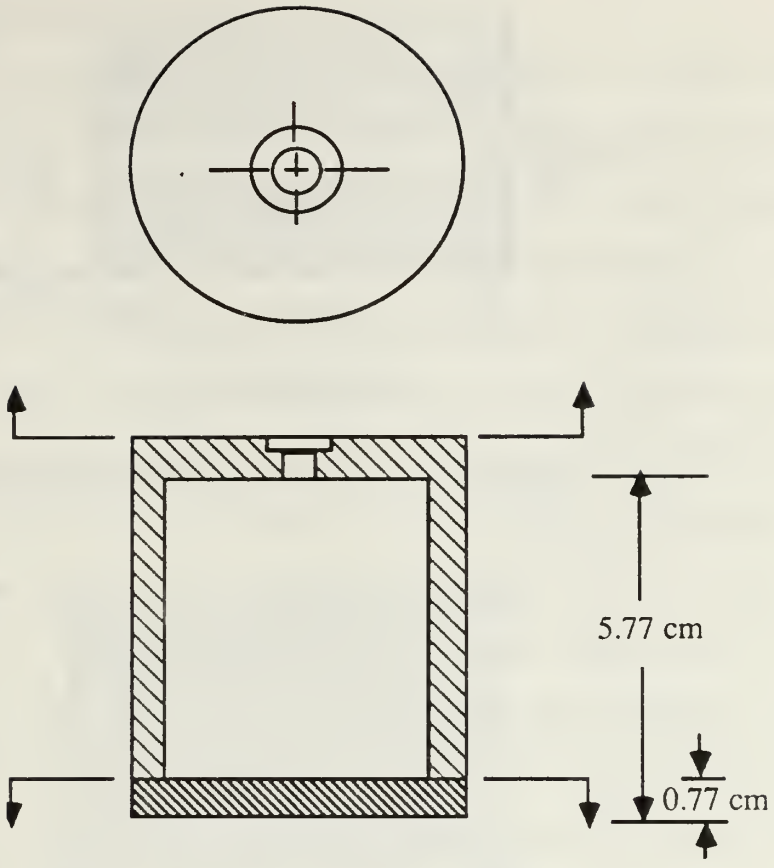

The Hot Heat Exchanger

$\Pi\Delta x = 0.0113\ m^2$

Figure 4 - The Nickel Heater Section

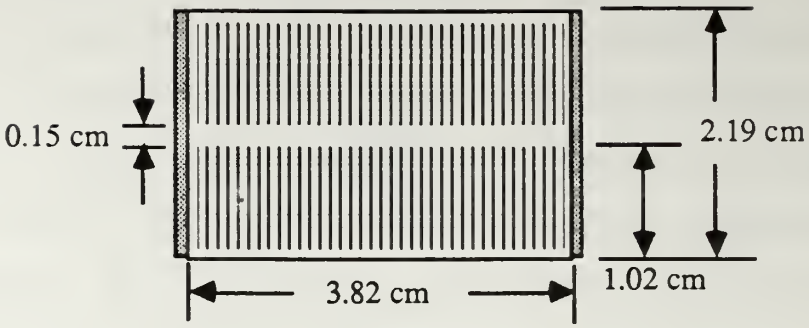

$\Pi\Delta x = 0.017\ m^2$

Figure 5 - The Ambient Heat Exchanger

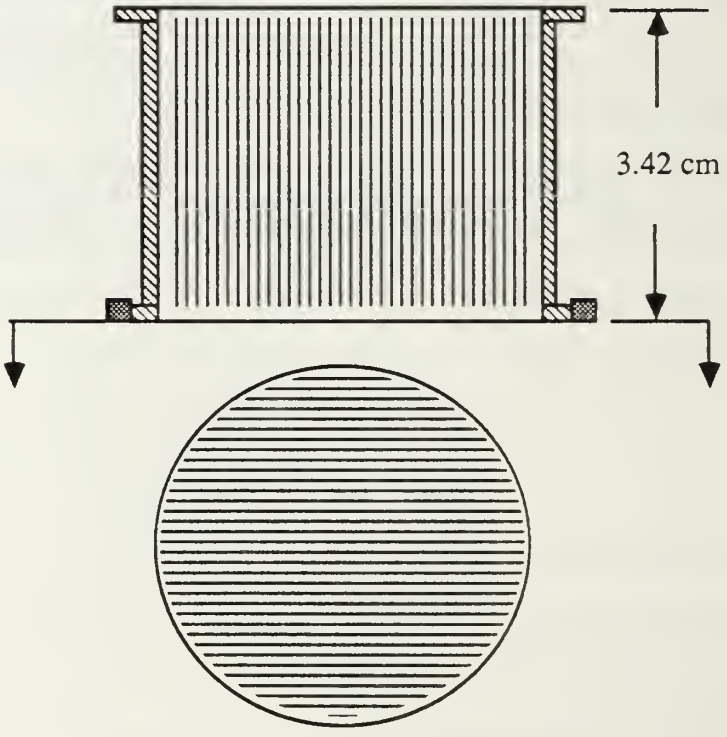

$\Pi\Delta x = 0.072\ m^2$

Figure 6 - Prime Mover Stack Container

C. TEMPERATURE CONTROL EQUIPMENT

Control of the temperature gradient across the prime mover stack is achieved by an OMEGA Model 9151 miniature microprocessor temperature controller, a HBA Model 202040 heater and a Neslab Model RET-110 constant temperature bath. The heater was mounted to surround the nickle heater section. As shown in Figure 7, output of the temperature controller was fed to a voltage divider and then connected to the Amplitude Modulation input of the function generator. Output from the function generator is then connected to the heater through a power amplifier. Water is circulated by the constant temperature bath through a water jacket which surrounds the ambient heat exchanger. The water pipe was also wrapped around the long section of the prime mover to maintain a uniform temperature. A type K thermocouple is soldered to the hot heat exchanger to sense the temperature of the hot end. Three type E thermocouples were glued to the top, middle, and bottom of the long section of the prime mover to sense the temperature along that section. The reference temperature for the whole system is found by using a 4-wire method to measure the resistance of a thermistor mounted on an isothermal aluminum block. It is difficult for an operator to monitor temperature using these thermocouples because their outputs give voltages rather than actual temperature. Therefore in order to monitor actual temperature directly, two type E thermocouples thermometers were glued on to the ambient heat exchanger container and the bottom of the prime mover. With this temperature control equipment, the maximum deviation of the applied temperature difference is 1 °C.

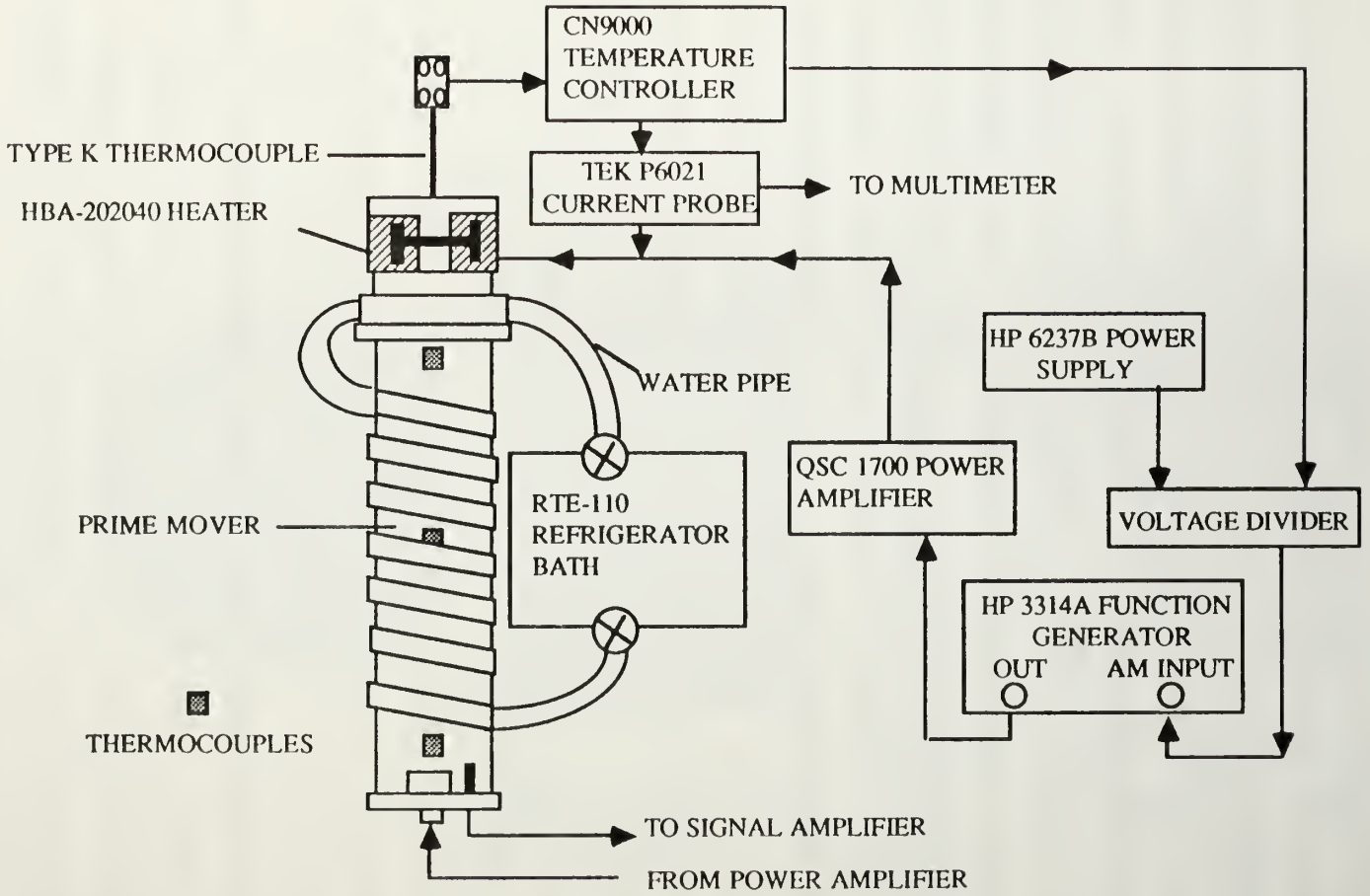

Figure 7 - Temperature control equipment

D. INSTRUMENTATION AND PROCEDURE

As discussed at the beginning of this chapter, the primary goal is to measure the quality factor of the prime mover. The measurement technique employed was to drive the prime mover at a frequency near resonance and measure the steady state amplitude of the microphone output signal. In this manner, the steady state frequency response was obtained. The Q is determined by a least squares fit of the ideal response to this data.

The measurements consisted of three phases. The first phase consisted of measuring the Q of the empty resonant tube. The purpose of this phase was to give confidence in the measurement technique. The second phase consisted of measuring the Q of the prime mover as a function of applied temperature difference below onset. The third and final phase consisted of measuring the waveform of the acoustic signal produced by the prime mover above onset. The instrumentation and procedure was for each of these three phases are discussed in this section.

1. The Empty Resonant Tube

The experimental setup is shown in Figure 8. The data acquisition is performed by an PC AT compatible computer. The computer communicated with the SR-530 lock-in amplifier, the HP 3457A multimeter and the HP 8904A multifunction synthesizer through a GPIB interface. Through the execution of the controlling program, a source signal is supplied by the function generator to the electret driver. The output voltage from the microphone was amplified by a custom-made signal amplifier. All data signals of interest were fed to a HP 3457A multimeter. The output of the HP 3457A was used as the data input to the

computer. A KIKUSUI COS6100A oscilloscope was used to monitor the input signal to the electret and the output signal from the signal amplifier.

Before the data acquisition is started, the valve connected to the tube is opened and the system is pumped down and refilled with helium to the desired pressure three times in order to purge undesired gases. An ASM Model 110 turbo helium leak detector is then used to ensure no leakage exists.

When the automatic data acquisition begins, the program initially takes voltages from the PX-304 pressure transducer and converts to actual pressure. Next, the approximate resonance frequency and the half power bandwidth are entered into the computer, which then determines the start and stop frequencies and the frequency increment. After the valve is closed the function generator is turned on and the data acquisition is started. The program sets the driving frequency and measures temperatures, frequency, X and Y (the real and imaginary part of the signal amplitude). It also calculates frequency increment and repeats the process. The time required to measure the frequency response is approximately 5 minutes.

As discussed earlier, the resonance behavior of the tube as a function of frequency is given by

$$P = A\left(\frac{f}{f_0}\right)^2 \left|\frac{\cot(kL)}{kL}\right|, \tag{21}$$

where P is the acoustic pressure of the tube, A is a scaling constant, and $kL=\pi[\omega/\omega_0+i/(2Q)]$. A least squares fit is performed to obtain f_0, Q, and A.

2. The Prime Mover below Onset

The setup is shown in Figure 7 (the same portion with Figure 8 is not shown here). The measurement was performed as follows: First, the measurement performed earlier with the simple resonant tube was repeated. After that measurement, the heater was mounted around the nickel heater section and then encased in insulating material. The temperature controller and the constant temperature bath were turned on and set with a specific temperature. After thermal equilibrium is achieved, the data acquisition is started. The magnitude of the input electrical power was determined by taking the product of the voltage and current. The current was measured through a Tektronix Model P6021 current probe.

Since the quality factor increases with temperature, the HP 8904 synthesizer was replaced by a HP 3325A function generator to get better frequency resolution. This measurement was repeated with increasing temperature until sound was generated.

3. The Prime Mover above Onset

This configuration (Figure 9) was built to observe the behavior of the sound generated above onset. The long section of the prime mover was replaced by a different section of identical length which has an ENDEVCO Model 8510B-5 piezoresistive pressure transducer screwed through the center of the end cap. The transducer is housed within another cap which is bolted to the end cap with brass flange. A high impedance leak is provided between the resonator and the back volume to eliminate dc pressure difference with little effect on acoustic pressure differences.

In this phase of the experiment, it was desired to measure the steady state electrical power input to the heater. This task was accomplished as follows: (1) the HP 3314A function generator was set up with a small constant voltage. (2) the controller was set to 900 °C to ensure the heater was turned on all the time. After reaching heat equilibrium i.e. the temperature of hot end is constant , the data acquisition is started. The output signal from the piezoresistive pressure transducer was amplified by an AM 502 differential amplifier and connected to a HP 3457A Multimeter and a HP 3561 Dynamic signal analyzer. A Tektronix Model 2445A oscilloscope was used to monitor the output signal and the dc voltage supplied to the differential amplifier.

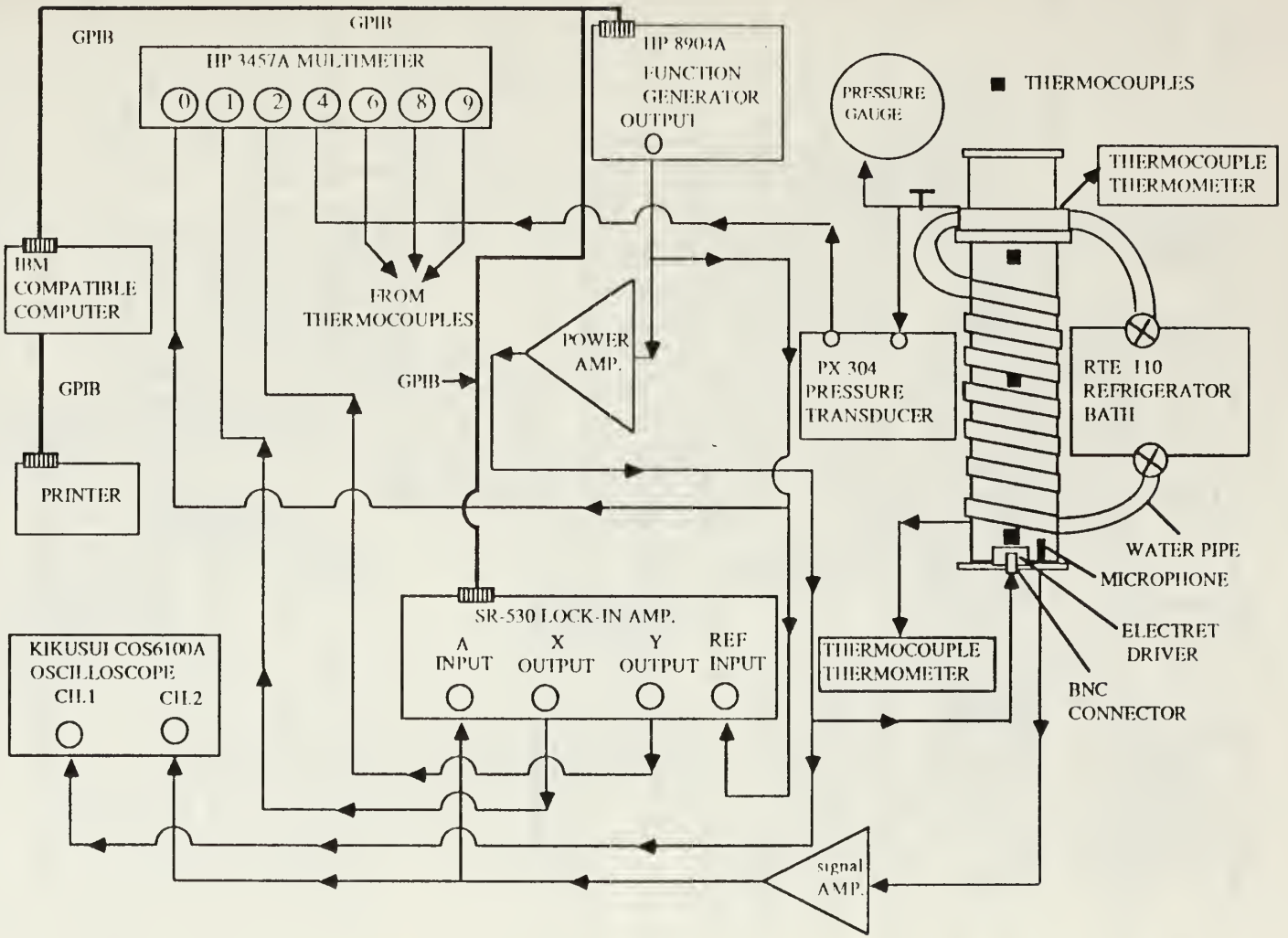

Figure 8 - Experiment setup of the resonant tube

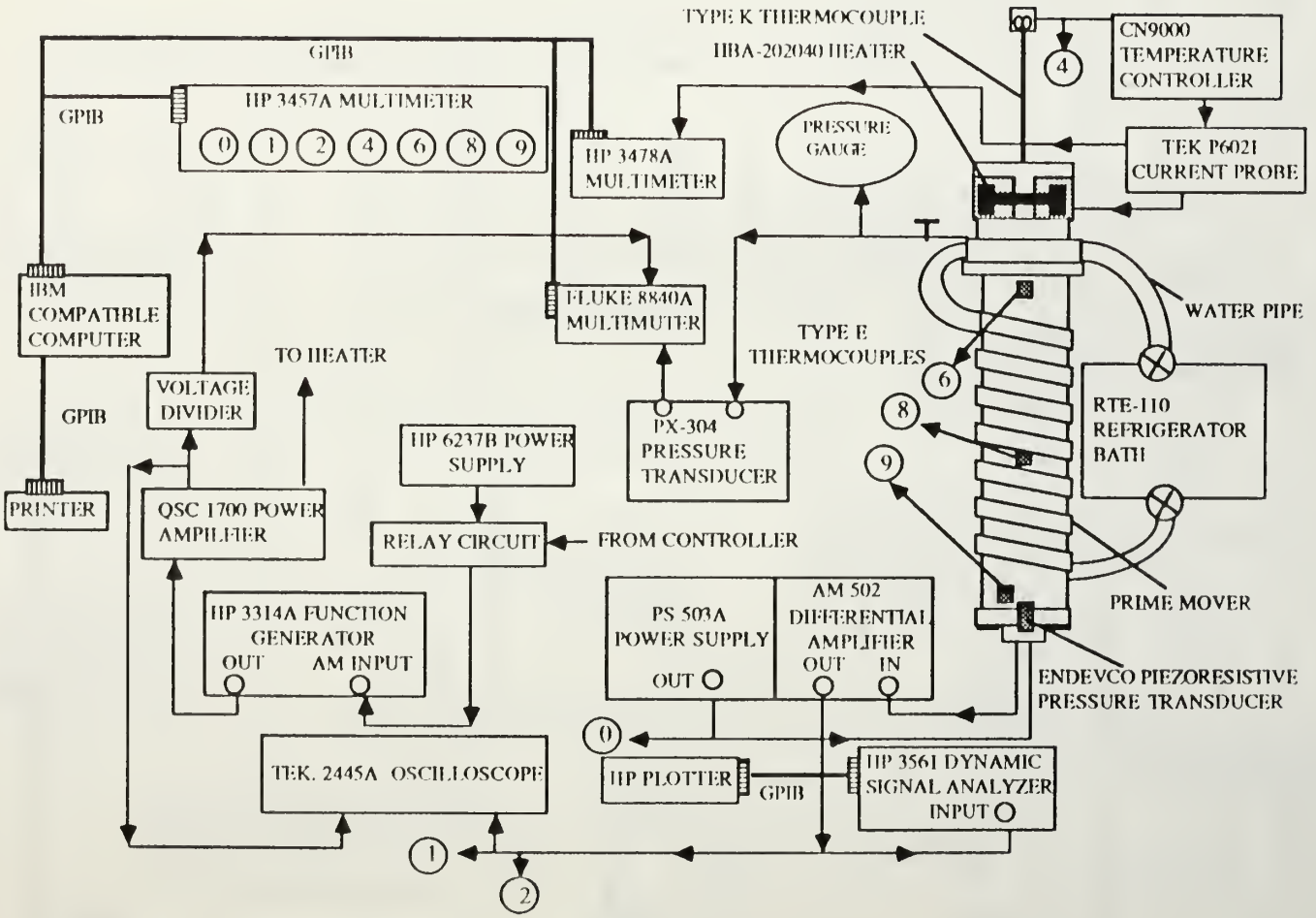

Figure 9 - Measurement setup above onset

IV. RESULTS AND DISCUSSIONS

The results of the three phases of the experiment will be presented and discussed in this chapter. The results for the empty resonator tube will be presented first, followed by those for the prime mover below onset. Finally, the results for the prime mover above onset will be presented.

Investigation of the empty resonator tube and the prime mover below onset both involve determining the resonance frequency and the quality factor from the measured frequency response. An example of the frequency response data is shown in Figure 10, which is a graph of the amplitude of the voltage output from the electret microphone as a function of drive frequency. Although this particular data set is for the prime mover with a 198 °C temperature difference across the stack, it is representative of the data obtained under all conditions. The solid curve represents the ideal response based on the fit to Equation 21. Also indicated in the figure are the estimated errors of the fitted resonance frequency and Q values.

A. THE EMPTY RESONANT TUBE

The Q's of the first three modes of the empty resonator were measured for mean gas pressure ranging from approximately 170 to 500 kPa. The results are plotted in Figure 11, which is a graph of Q versus the square root of the mean gas pressure. The square root of the mean gas pressure was chosen as the abscissa because, as seen from Equation 16, $Q \propto 1 / \delta_v \propto P_m^{1/2}$. The solid lines represent the theoretical Q as computed from Equation 16. In general the agreement is quite good, although there is a tendency to slightly over predict the

Q, indicating the presence of unaccounted losses. Two measurements were made at each pressure. In all but a few cases the two results fall on top of one another. The estimated error of the fit is no larger than the size of the symbols representing data points.

An indication of how closely the empty resonator behaves to an ideal, rigidly terminated tube is given in Figure 12. The ordinate of this graph is the ratio of the measured (fitted) resonance frequency to the ideal frequency $f = nc/2L$, computed using $c = 1008\ ms^{-1}$ (the sound speed of helium at 20 °C) and $L = 1.02 \pm 0.01$ m. As seen, all of the values are within 2 to 3% of 1.00. An error of approximately 0.4 % can be attributed to the fact that the actual temperature of resonator during the measurements was closer to 18 °C than 20 °C. An additional source of error may be due to the fact that the total length of 1.02 m was arrived at by adding the individual lengths of the ambient end, the ambient heat exchanger container, and the hot end measured separately before the resonator was assembly by soldering the three parts together. If the three parts did not fit together exactly, the actual length of the resonator may have been slightly longer than the unassembled length.

B. THE PRIME MOVER BELOW ONSET

The results of the measurements of the Q of the prime mover's fundamental mode below onset for five different mean gas pressures are presented in Figures 13 through 17, which show 1/Q as a function of the temperature difference across the stack. The solid line represents the theoretical prediction using Equation 6 and 11 through 14, which are based on the boundary layer assumption and the short stack approximation. The calculation of the contributions from the ambient and hot end is straightforward. The

thermophysical properties of the gas are computed using either the ambient or hot end temperature, whichever is appropriate. In order to calculate the contributions from the heat exchangers, x in Equation 13 is set equal to the location of the center of the heat exchanger, and again the thermophysical properties of the gas are computed using either the ambient or hot end temperature, whichever was appropriate. In order to compute the contribution from the stack, x in Equation 14 is set equal to the location of the entrance to the stack. The temperature gradient across the stack is accounted for in the following manner. Other than the propagation constant, the only temperature dependent quantities in Equation 14 are the thermal and viscous penetration depths. In order to account for their temperature dependency, Equation 14 is converted into a differential by replacing Δx by dx. By assuming a linear temperature gradient across the stack, the temperature dependence of the penetration depths can be converted into an x dependence. The reciprocal of the Q is computed by numerically integrating the differential form of Equation 14, with x-dependent penetration depths, along the length of the stack. The interpretation of this computation is that, in the short stack limit, the acoustic parameters in the stack are determined by their values at the stack entrance. The only modification necessary is to adjust the particle velocity for the presence of the stack and the viscous boundary layer.

Before the integration of the penetration depth can be accomplished, it is necessary to determine its temperature dependence. This dependence is found by performing a least squares fit to viscosity and thermal conductivity data obtained from an NBS table [Ref. 6]. The result for both the thermal and viscous penetration depths in helium is that $\delta \propto T^{0.85}$.

There are several important features evident in Figures 13 to 17. The overall agreement is good, through the quality of the agreement diminished with decreasing mean gas pressure. In each case, there is a tendency to over predict the losses at low temperature difference. Finally, at the lower values of gas pressure, the data tend to tail off near onset, a feature not predicted by the theory.

In order to understand the discrepancies discussed above, the validity of the approximations must be investigated. For the fundamental mode, the short stack approximation is well satisfied because the length of the prime mover stack is only about 10 % of the radian wavelength. As for the boundary layer assumption, the penetration depth for the average stack temperature is plotted as a function of the temperature difference in Figures 17 and 18. If $y_o/\delta_\kappa \geq 1.5$ the boundary layer approximation is valid. For the viscous penetration depth, at high mean gas pressure the boundary layer assumption is well satisfied, but this assumption starts to fail when the mean gas pressure decreases. The boundary layer assumption for the thermal penetration depth is not satisfied very well at any pressure.

In order to determine if there is any connection between the failure of the boundary layer approximation and the tailing off of the data at low gas pressures, the 1/Q data are replotted in Figures 20 through 24. The solid lines in these figures represent a linear least squares fit to the low temperature difference data, where the viscous boundary layer approximation is valid. These lines fit the 500, 376, and 308 kPa data well over the entire range of temperature differences, as might be expected from the fact that the boundary layer approximation is valid in these cases at almost all temperature differences below

onset. However, the 239 and 170 kPa data begin to depart from the straight lines at an approximate temperature difference of 200 and 100 °C, respectively. Referring to Figure 18, these are the same points where the approximation begins to fail.

The results for the second and third modes of the prime mover are given in Figure 25 through 28 with two different pressures of 308 kPa and 170 kPa. The agreement is not very good, probably because the short stack approximation is violated at high modes. In the second and third modes the prime mover stack is 20 and 30 % of the radian wavelength. Although the quantitative agreement is poor, the theory does predict the correct dependence of 1/Q at $\Delta T = 0$ and ΔT at onset.

C. THE PRIME MOVER ABOVE ONSET

This final series of data contains the results above onset for the prime mover. Figures 29 and 30 show the waveform and the spectrum of the sound generated by the prime mover above onset. The mean gas pressure is 307 kPa. The temperature difference across the stack is 325 °C which is slightly above onset. The signal exhibits slight distortion, particularly in the positive cycle (Figure 29). Figure 30 shows that the difference in spectrum level between the first few modes is larger than 15 dB. Figures 31 and 32 show results for a temperature difference of 368 °C. The signal is distorted even further and there is more energy stored in high modes. At a temperature difference of 453 °C, the signal (Figure 33) is distorted sharply in both positive and negative half-cycles. Figure 34 illustrates the spectrum for the same signal. The difference in spectrum levels between for the first few modes has decreased further to less than 6 dB and more energy has been spread to higher modes.

The signals shown in these figures have very high amplitude. The peak positive pressure in Figures 29, 31, and 33 are approximately 3.3, 13.5, and 24.2 kPa, respectively. These amplitudes correspond to approximately 1.1, 4.4 and 7.9% of mean gas pressure.

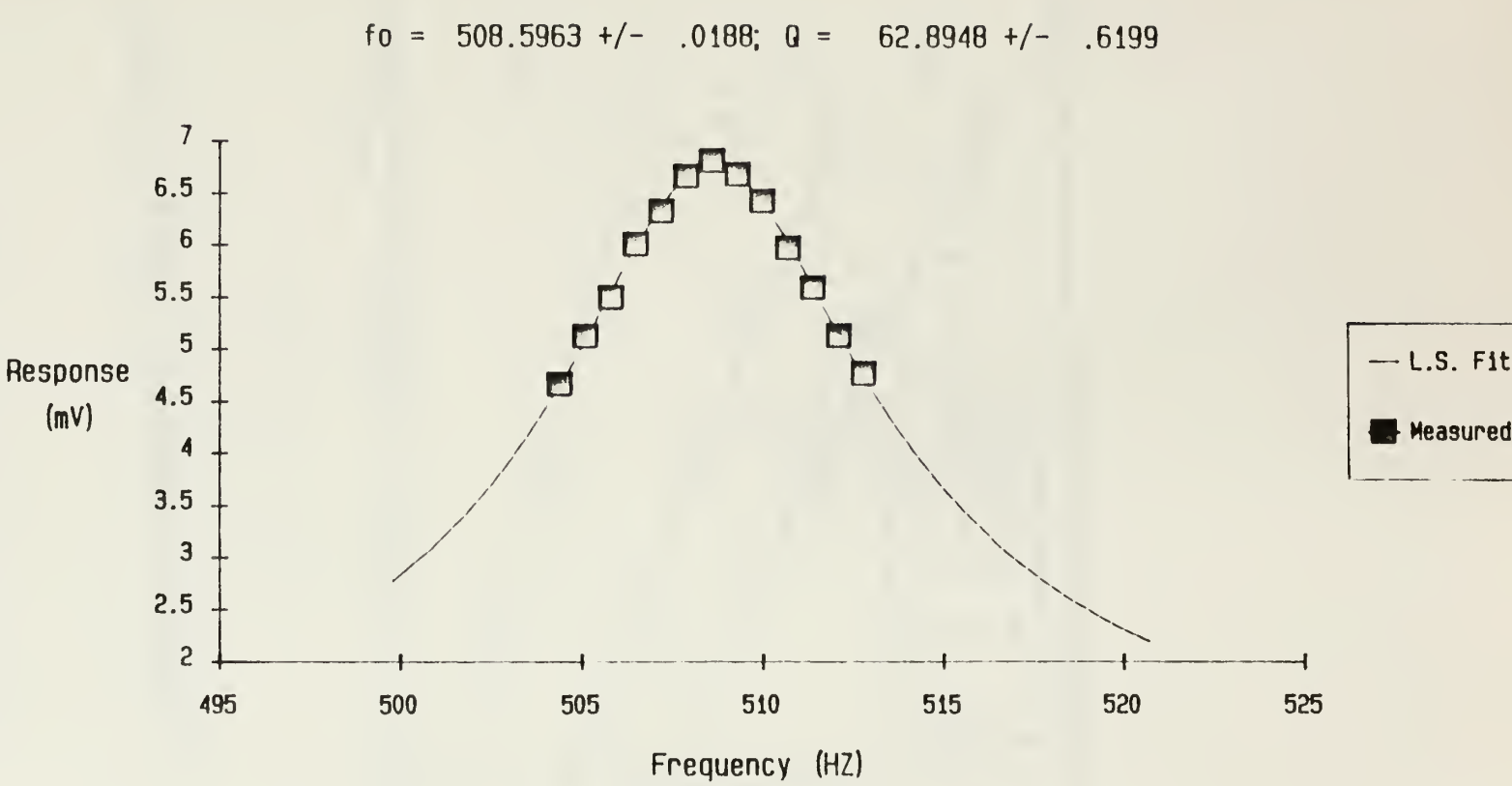

Figure 10 - A typical least squares fit of Q

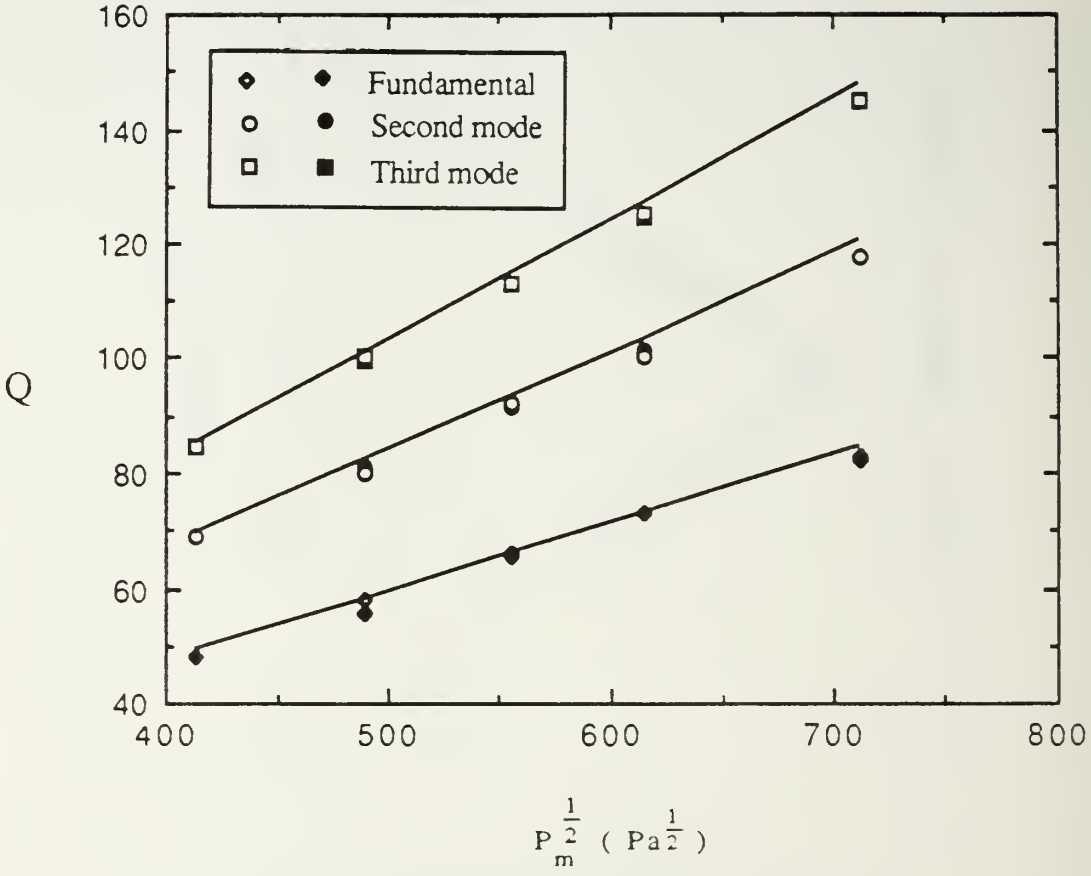

Figure 11 - Resonant tube with helium

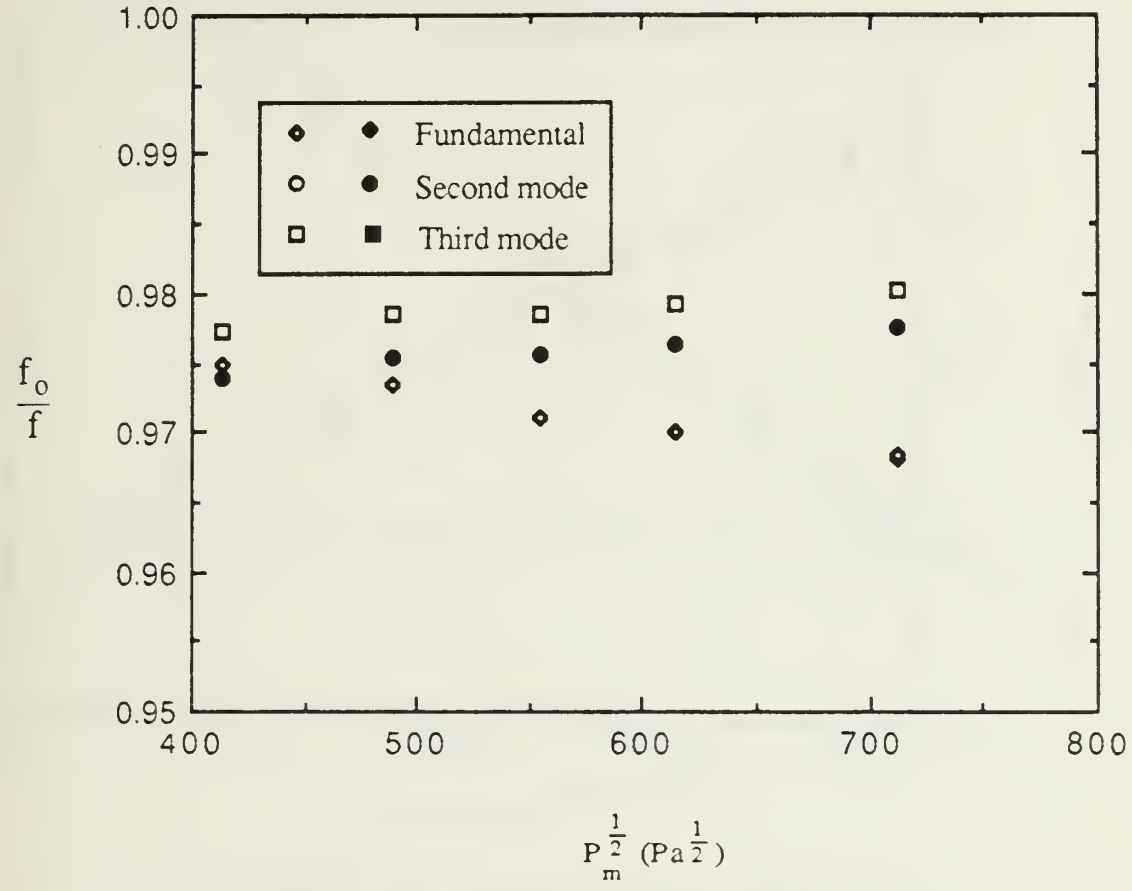

Figure 12 - Resonant tube with helium

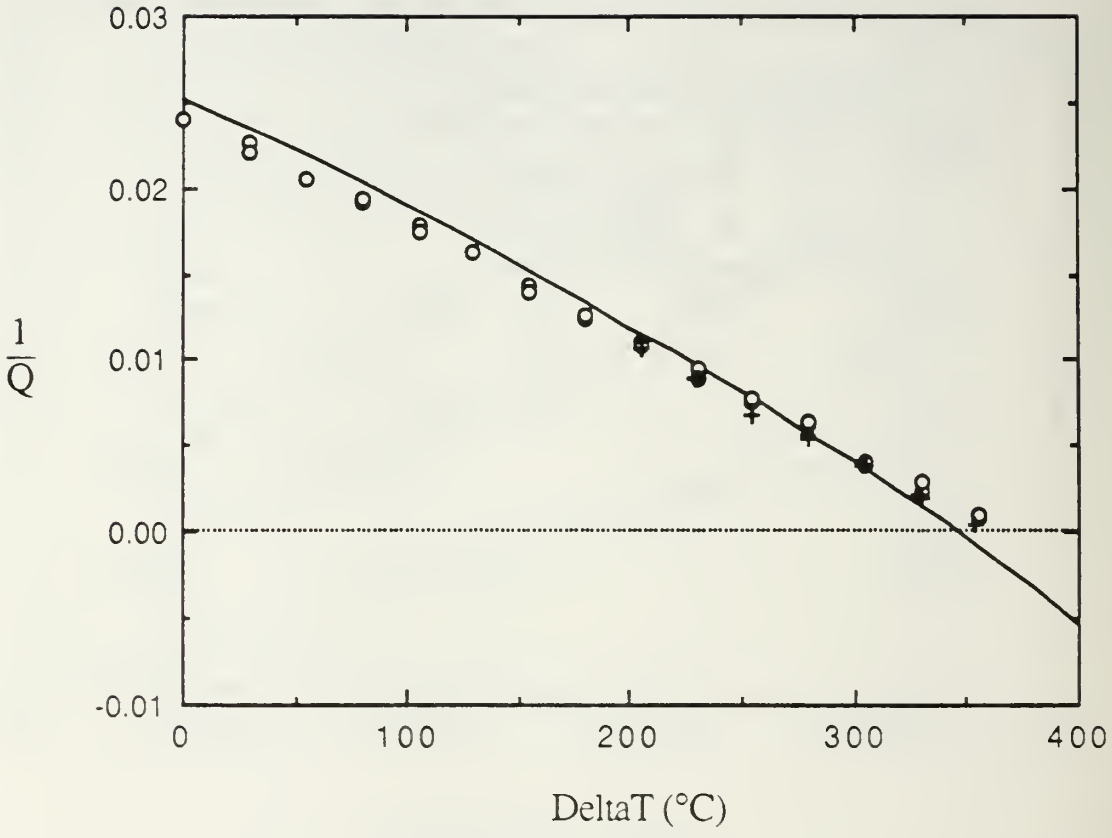

Figure 13 - Prime mover with helium at 500 kPa (the fundamental mode)

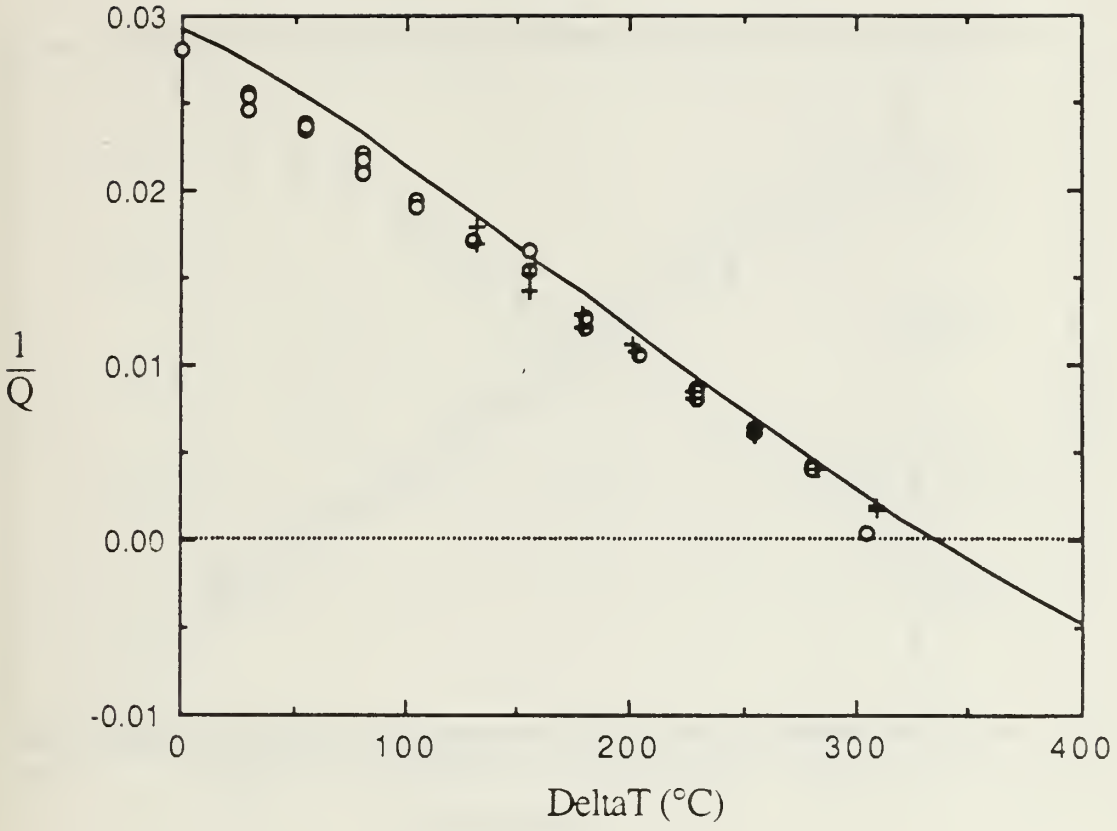

Figure 14 - Prime mover with helium at 376 kPa (the fundamental mode)

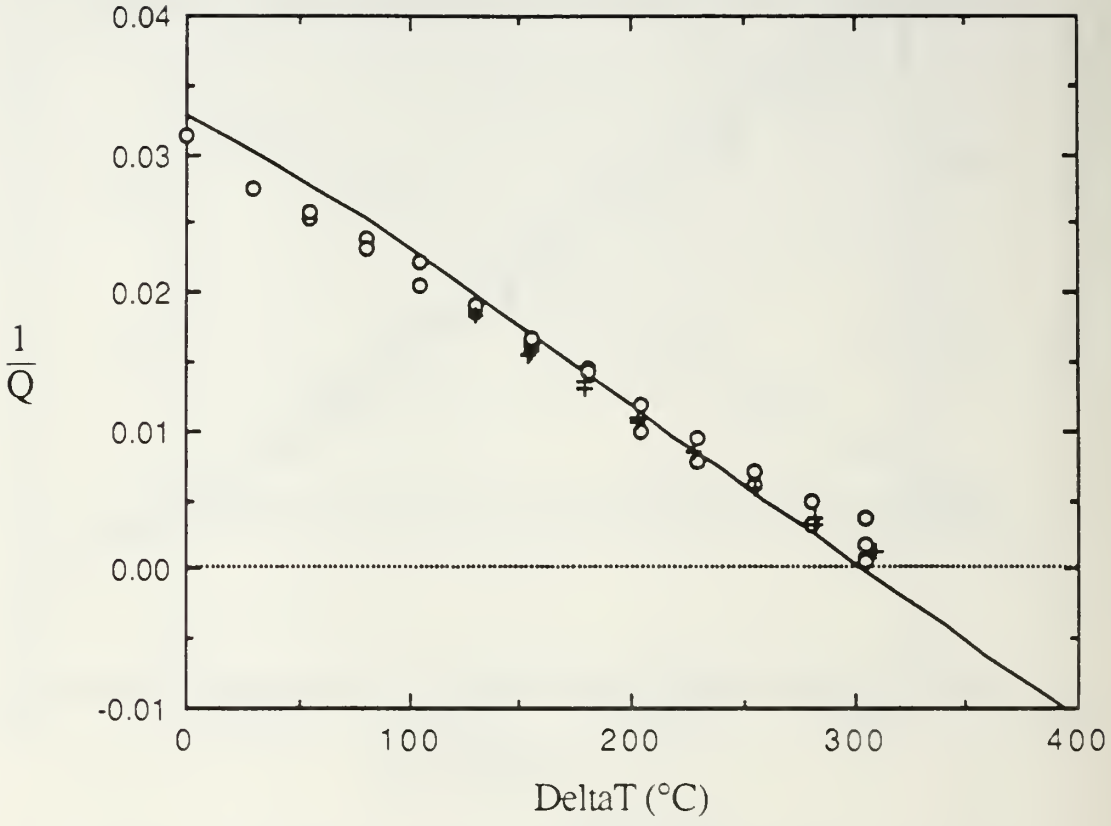

Figure 15 - Prime mover with helium at 308 kPa (the fundamental mode)

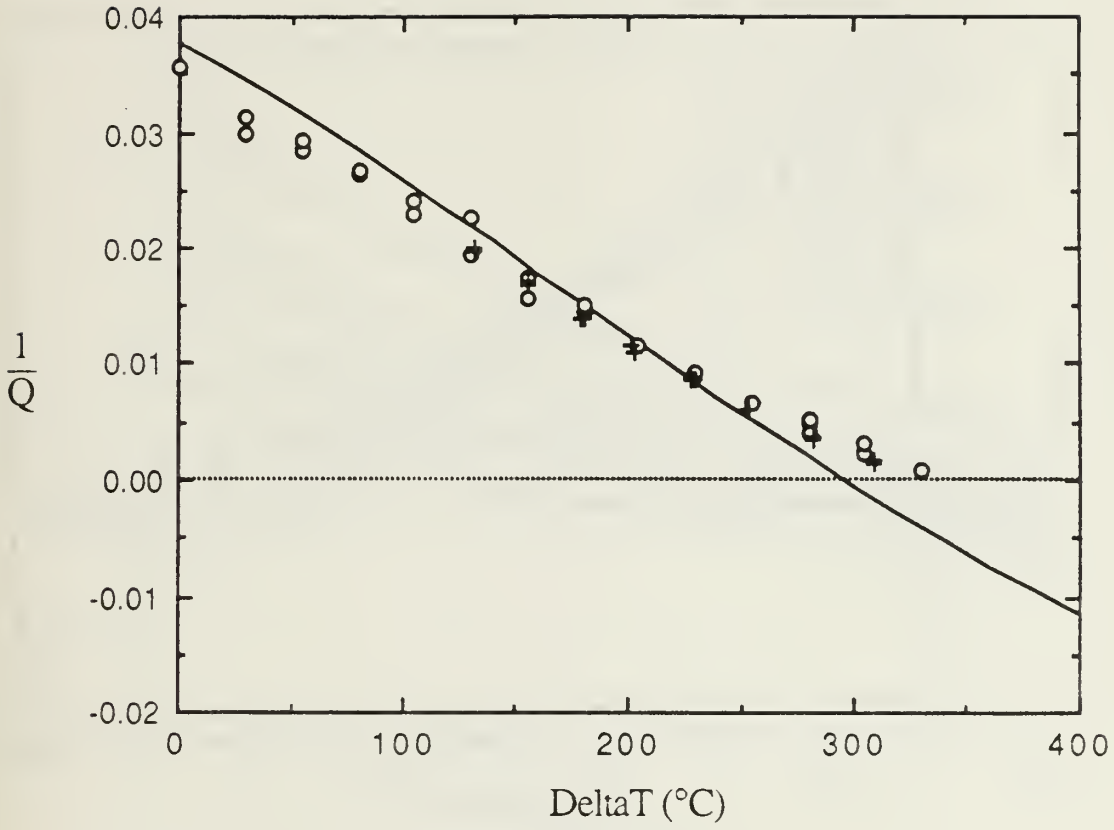

Figure 16 - Prime mover with helium at 238 kPa (the fundamental mode)

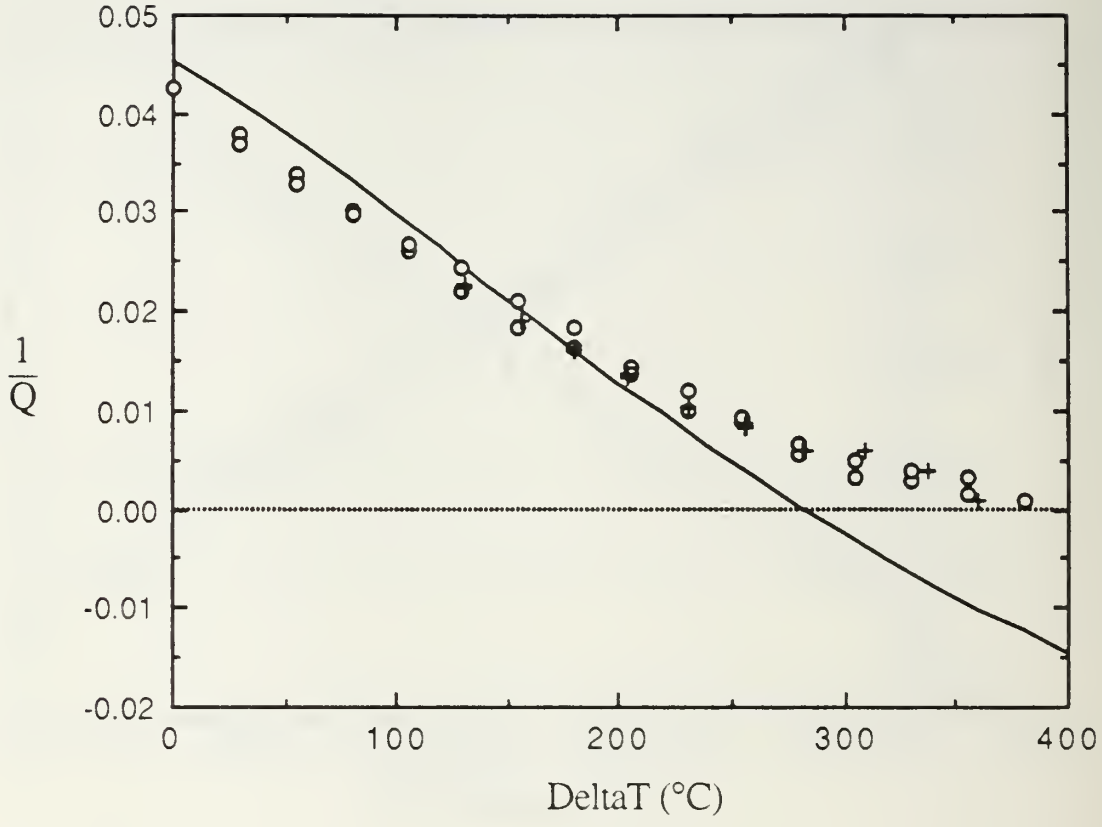

Figure 17 - Prime mover with helium at 170 kPa (the fundamental mode)

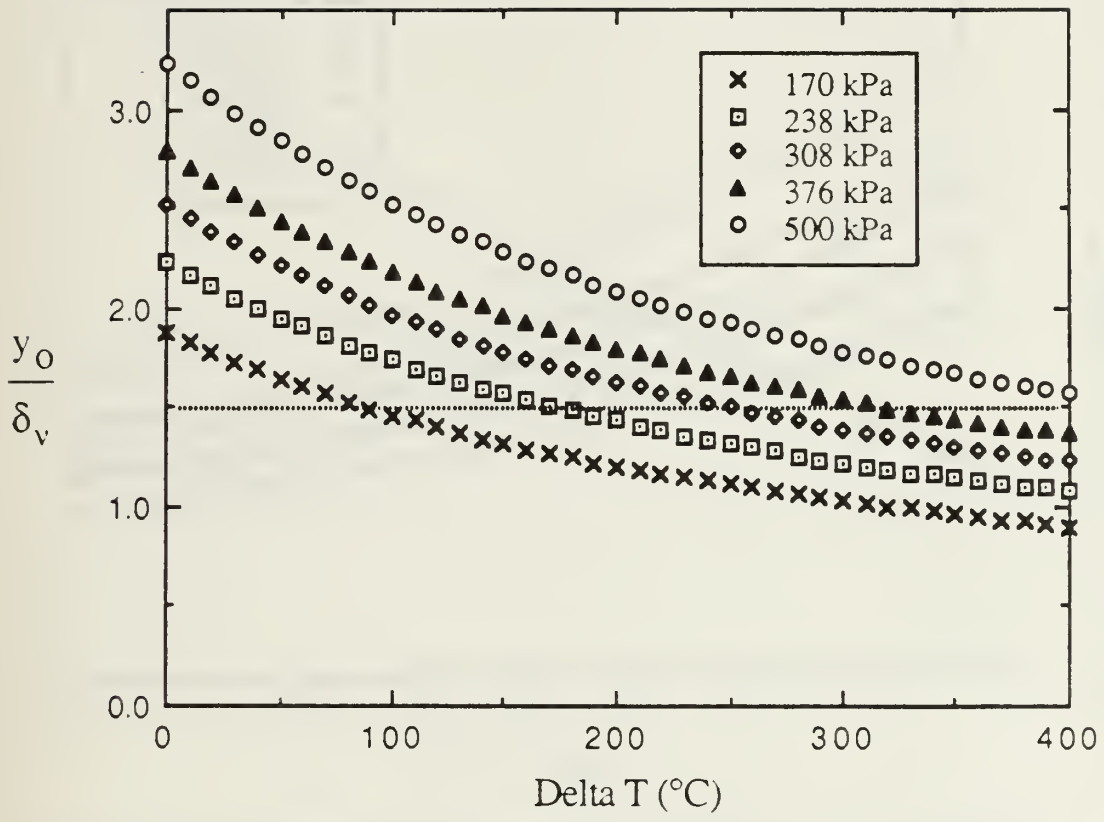

Figure 18 - Ratio of the plate half-gap to the viscous penetration depth Vs. temperature difference

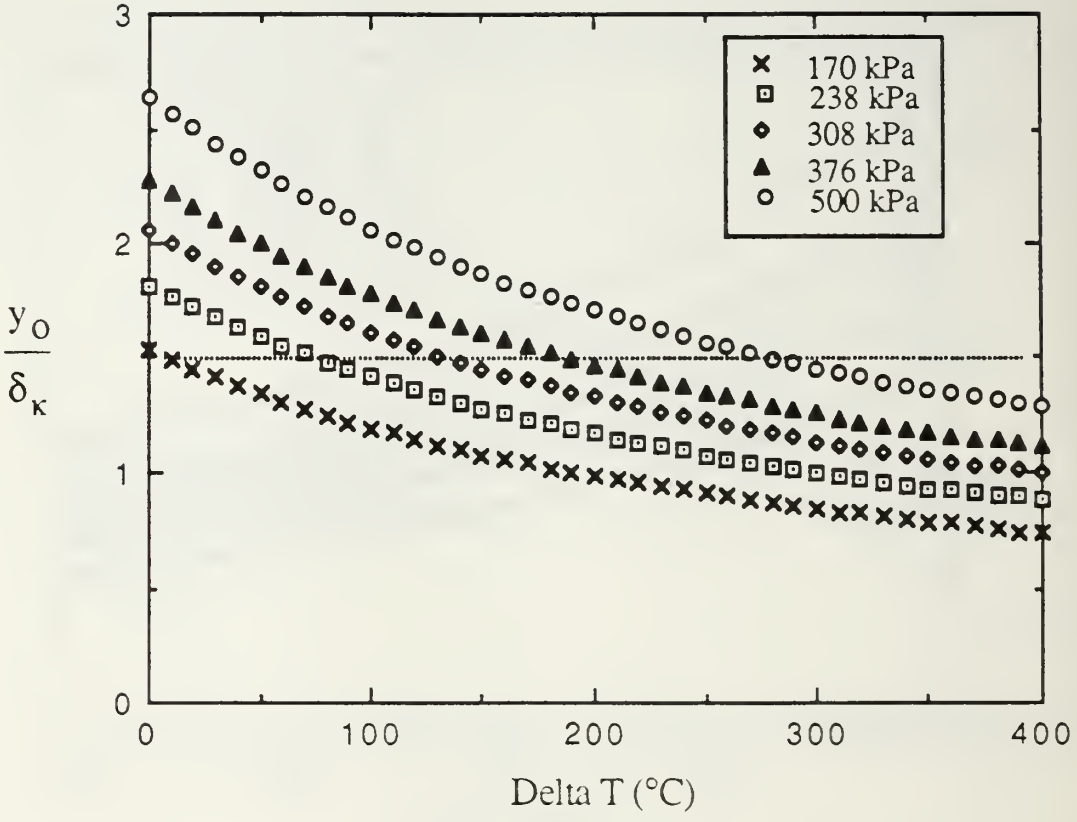

Figure 19 - Ratio of the plate half-gap to the thermal penetration depth Vs. temperature difference

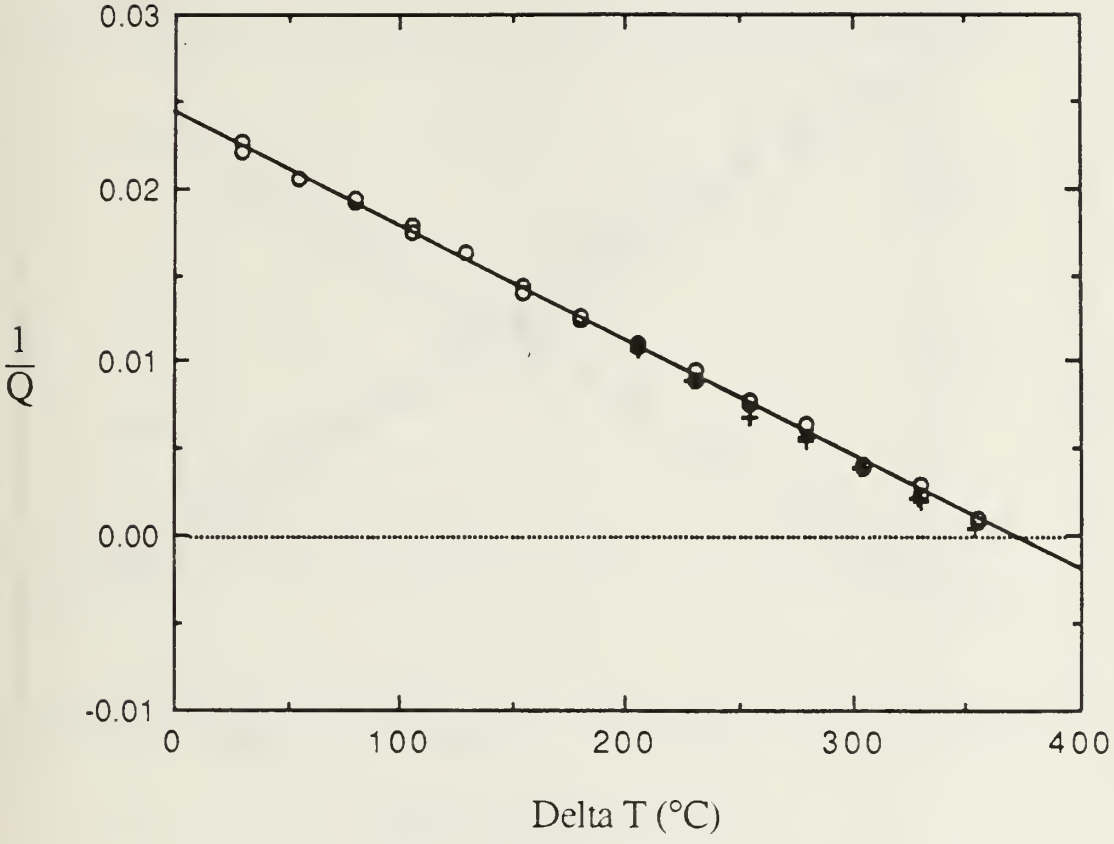

Figure 20 - Prime mover with helium at 500 kPa (the fundamental mode)

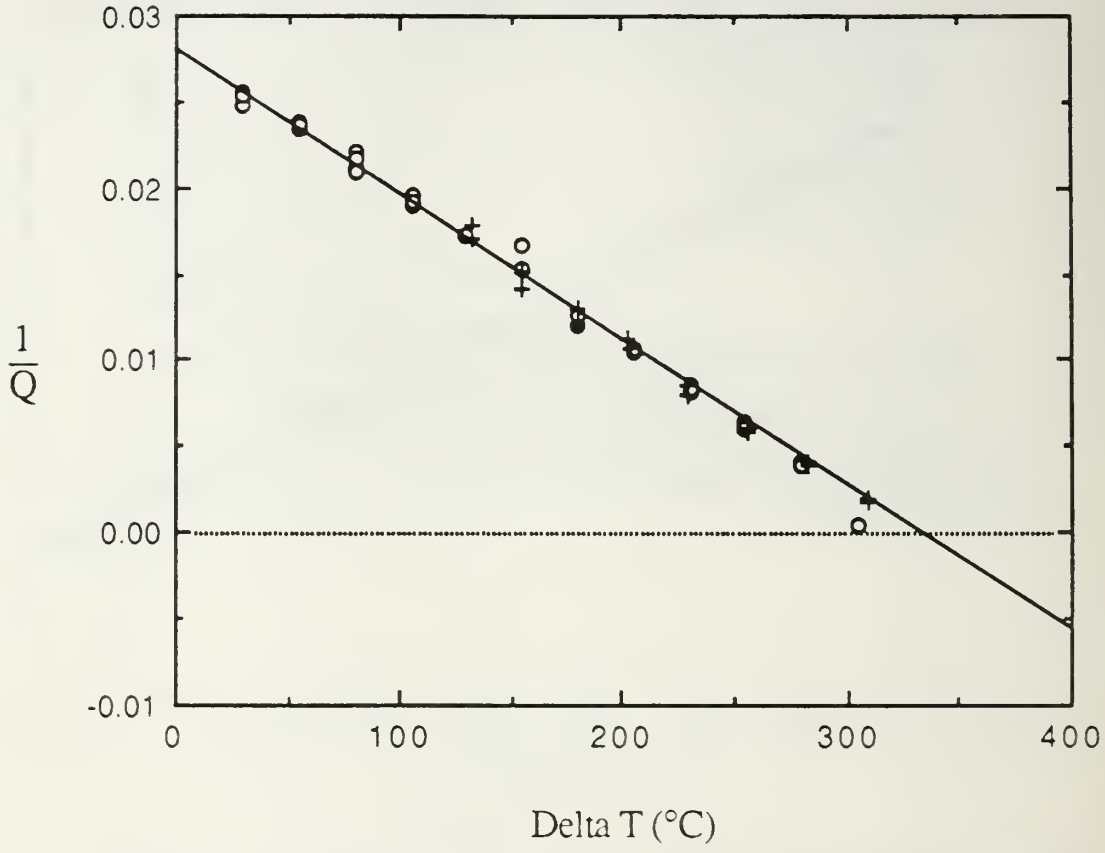

Figure 21 - Prime mover with helium at 376 kPa (the fundamental mode)

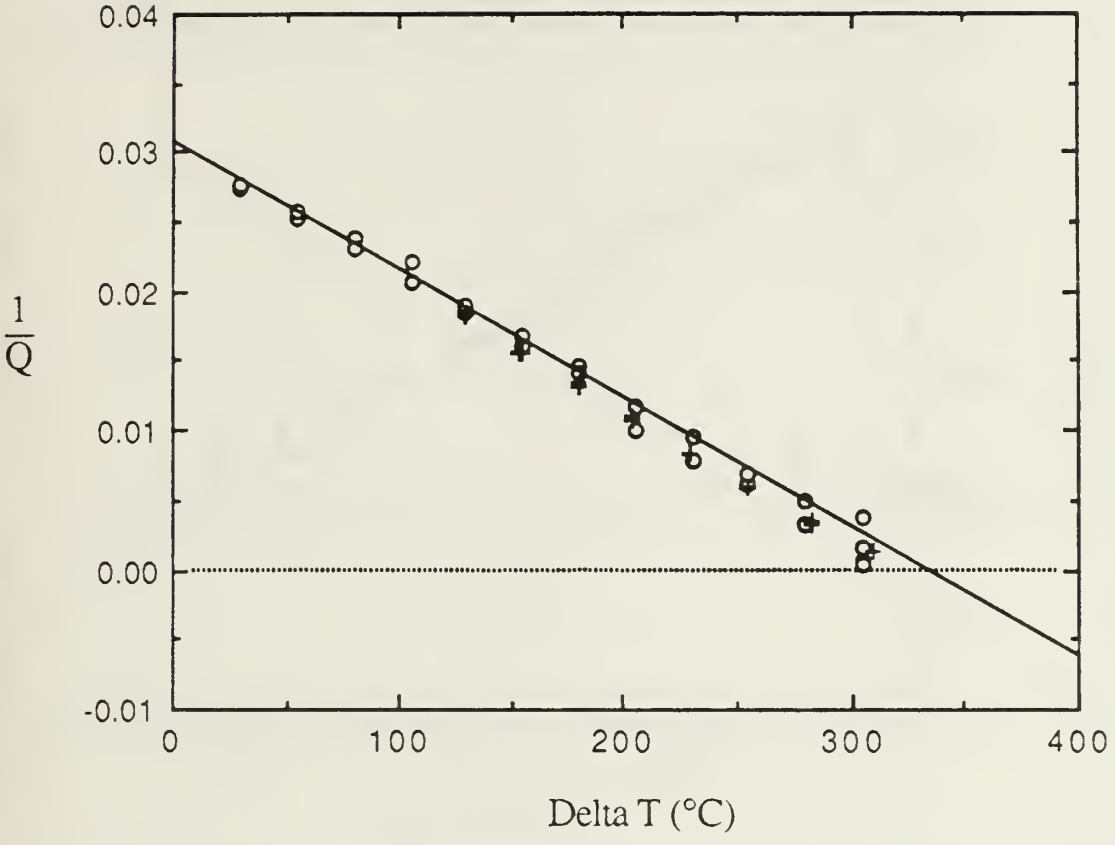

Figure 22 - Prime mover with helium at 308 kPa (the fundamental mode)

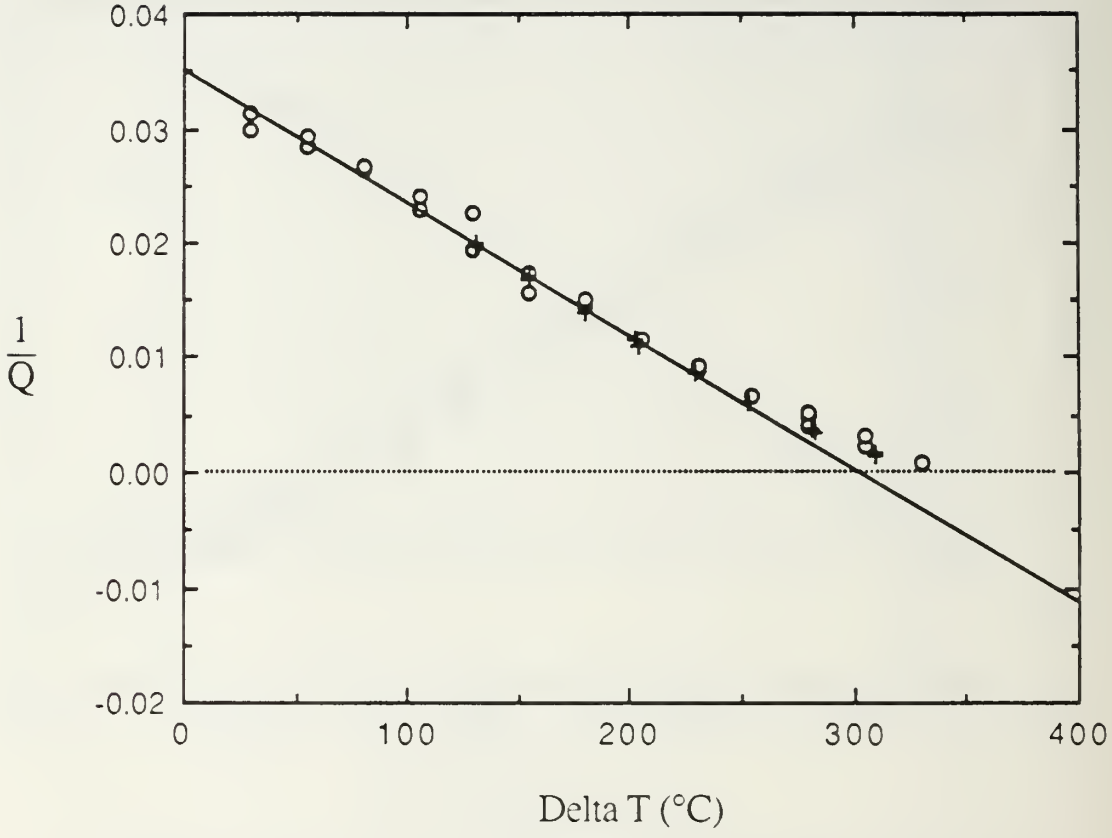

Figure 23 - Prime mover with helium at 238 kPa (the fundamental mode)

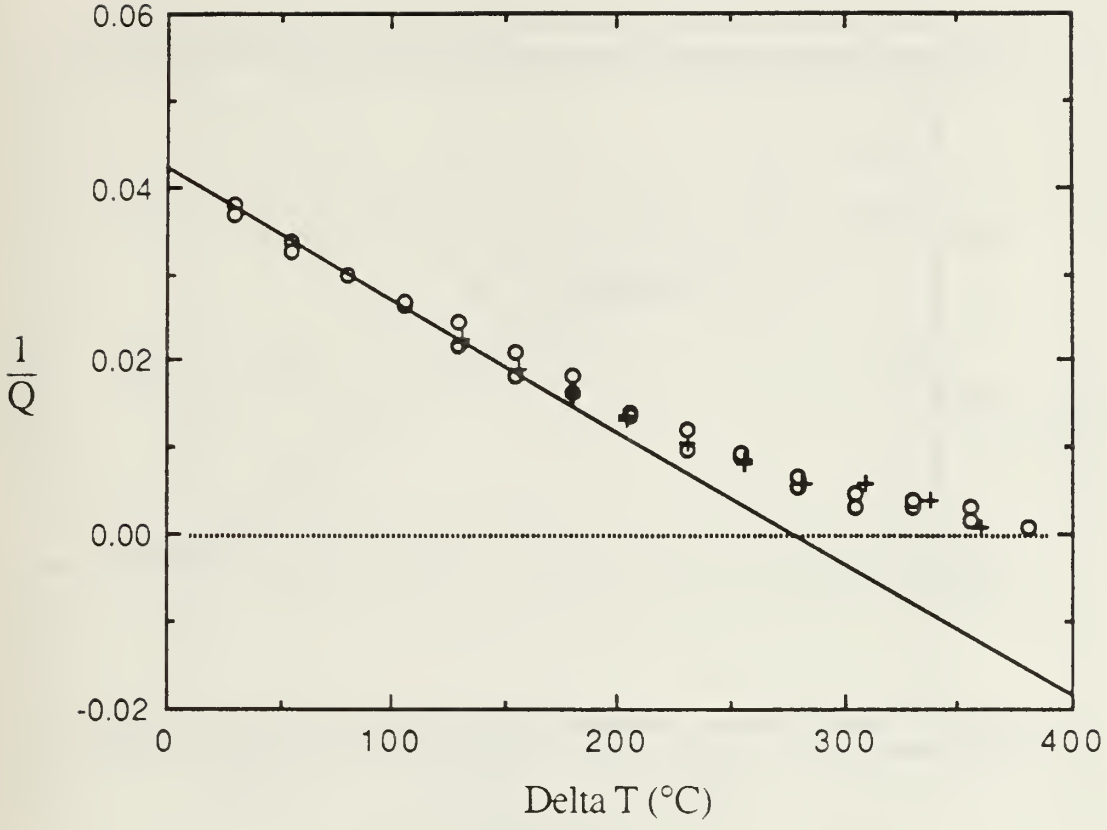

Figure 24 - Prime mover with helium at 170 kPa (the fundamental mode)

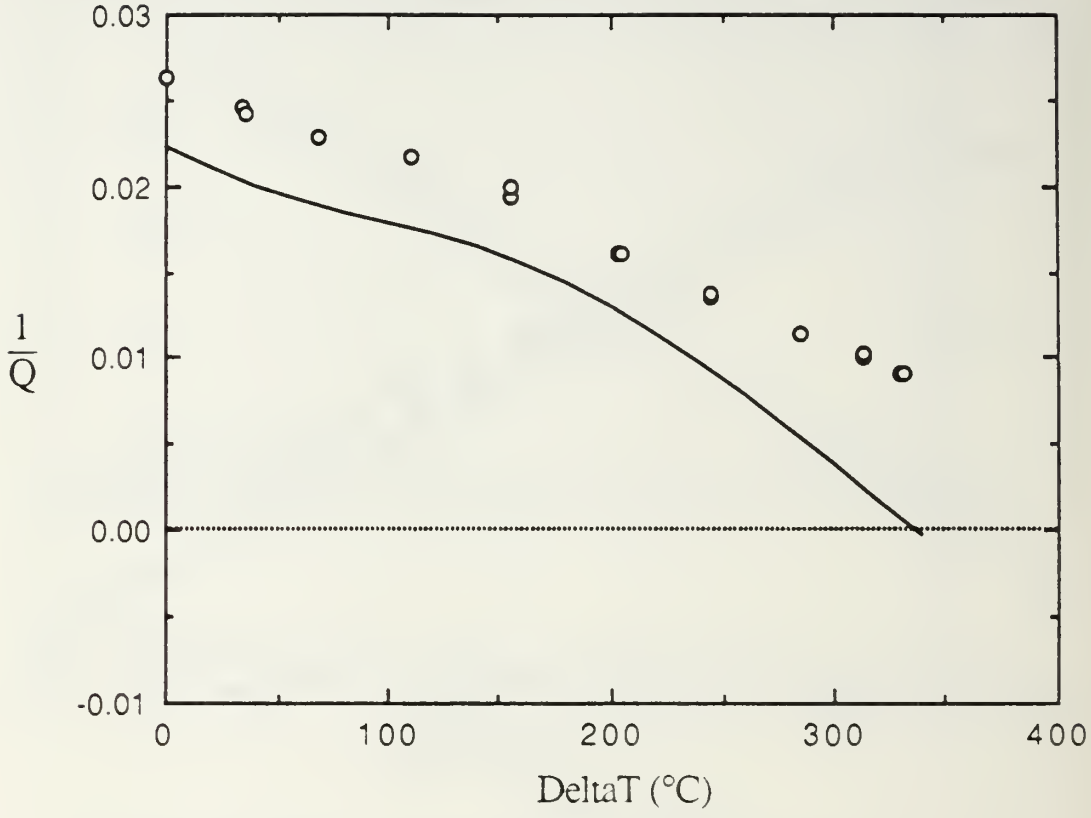

Figure 25 - Prime mover with helium at 308 kPa (the second mode)

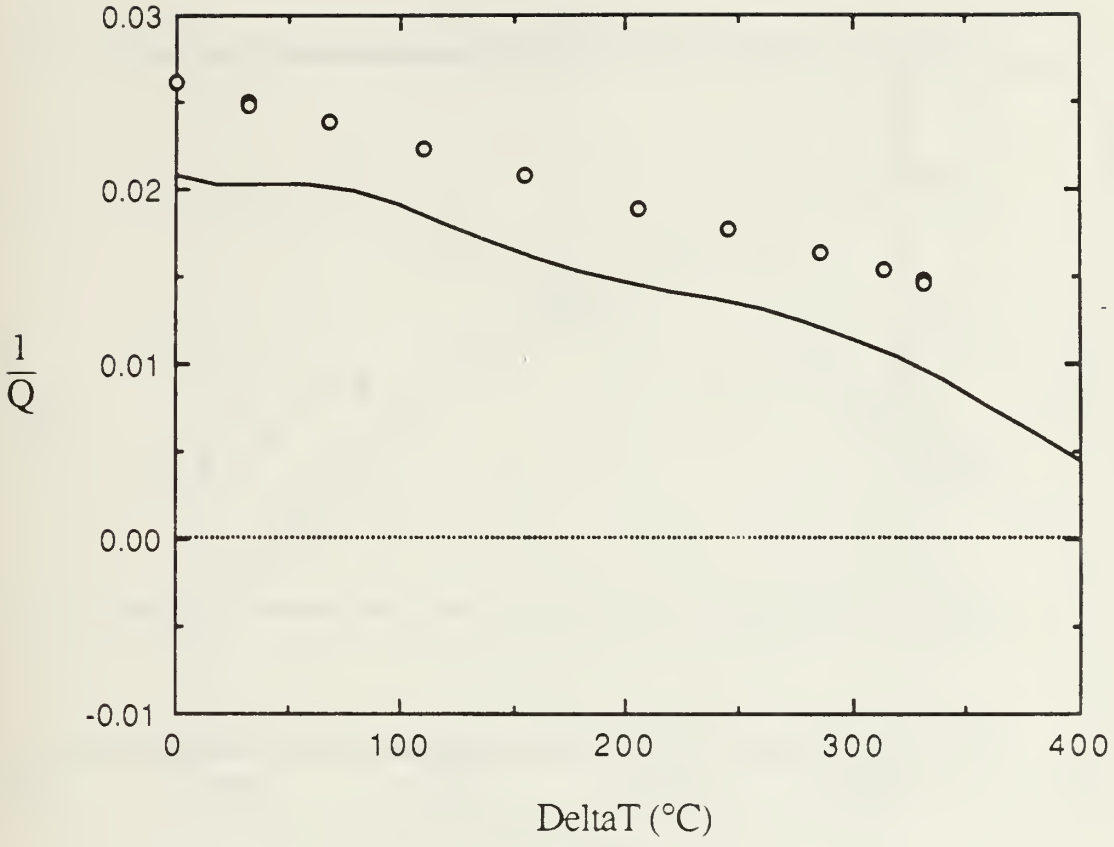

Figure 26 - Prime mover with helium at 308 kPa (the third mode)

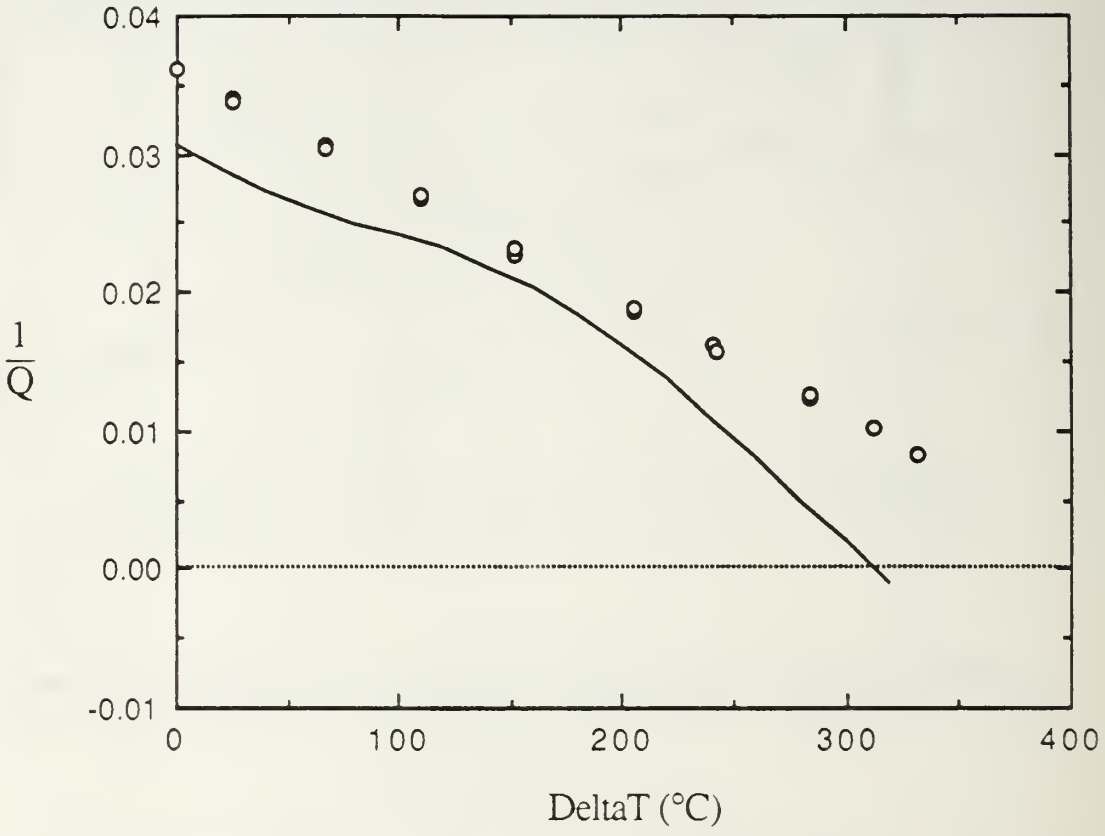

Figure 27 - Prime mover with helium at 170 kPa (the second mode)

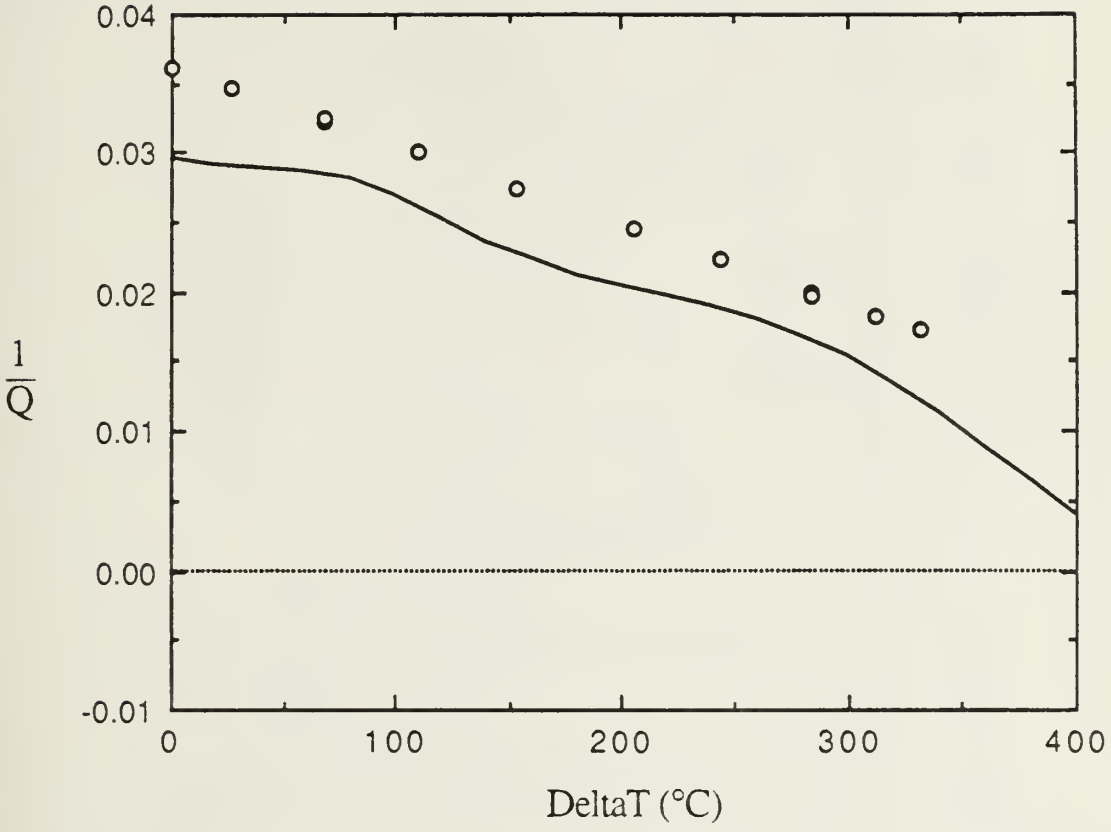

Figure 28 - Prime mover with helium at 170 kPa (the third mode)

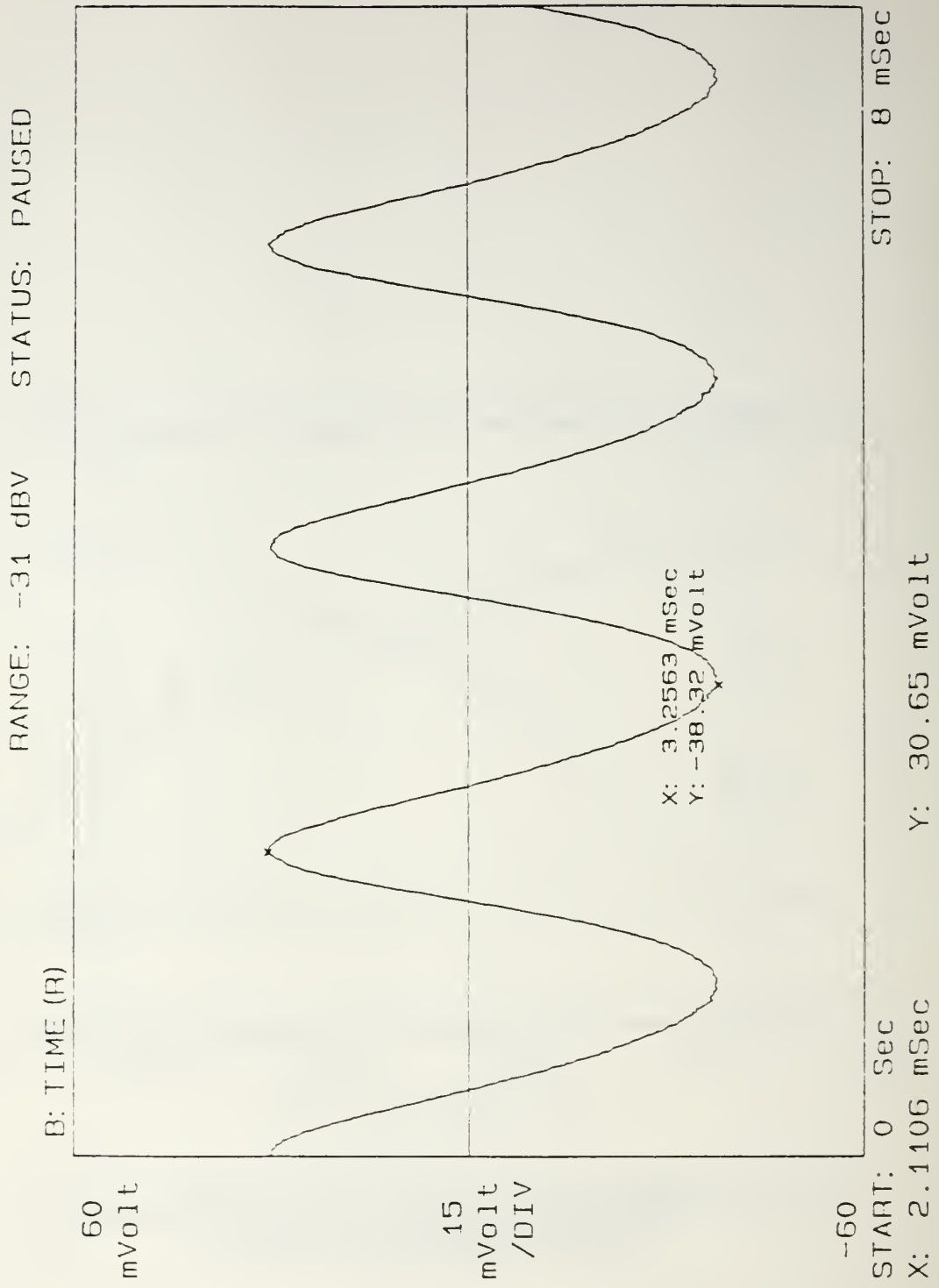

Figure 29 - Waveform of the sound generated by the prime mover at a temperature difference of 325 °C

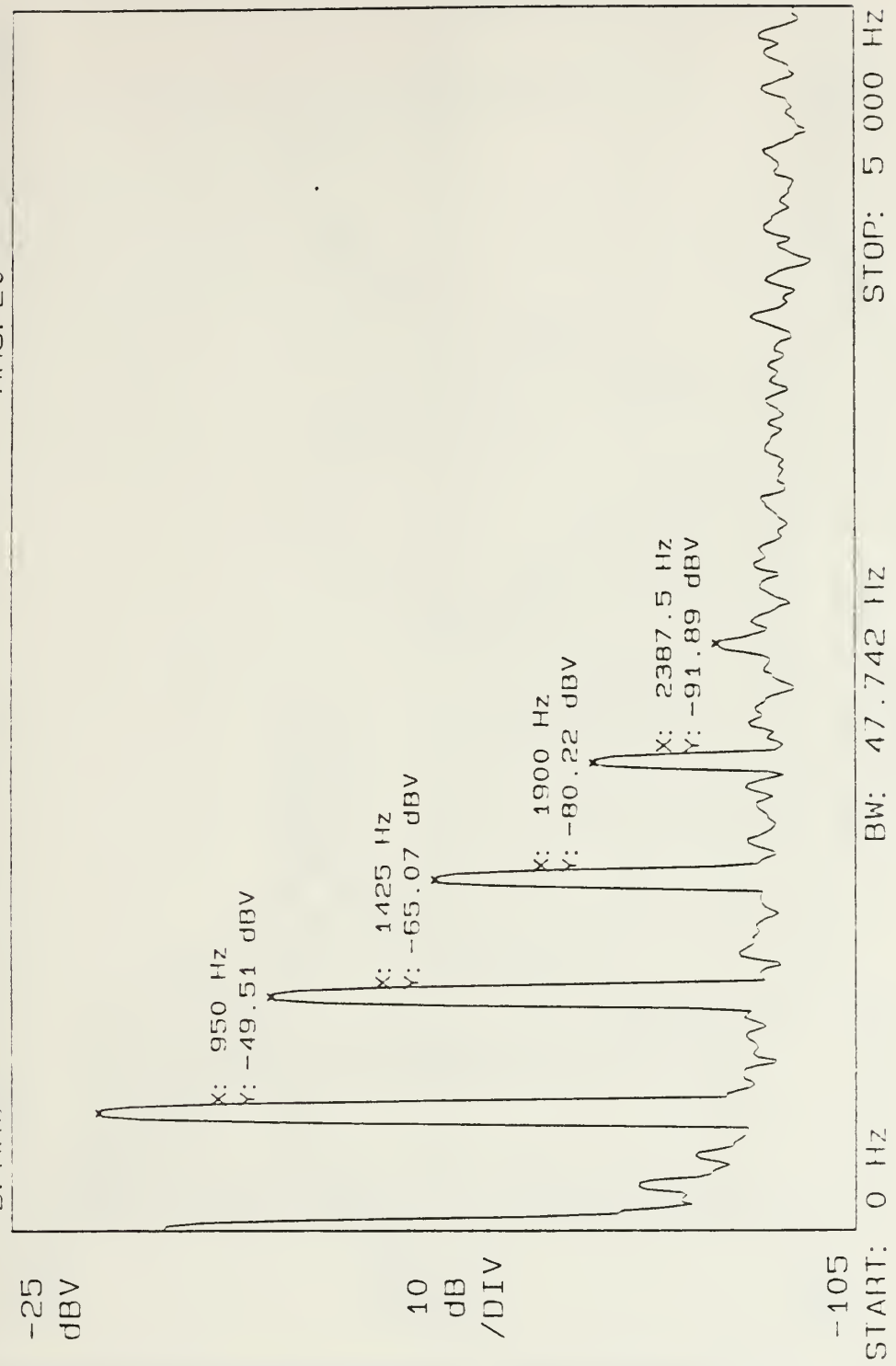

Figure 30 - Spectrum of the sound generated by the prime mover at a temperature difference of 325 °C

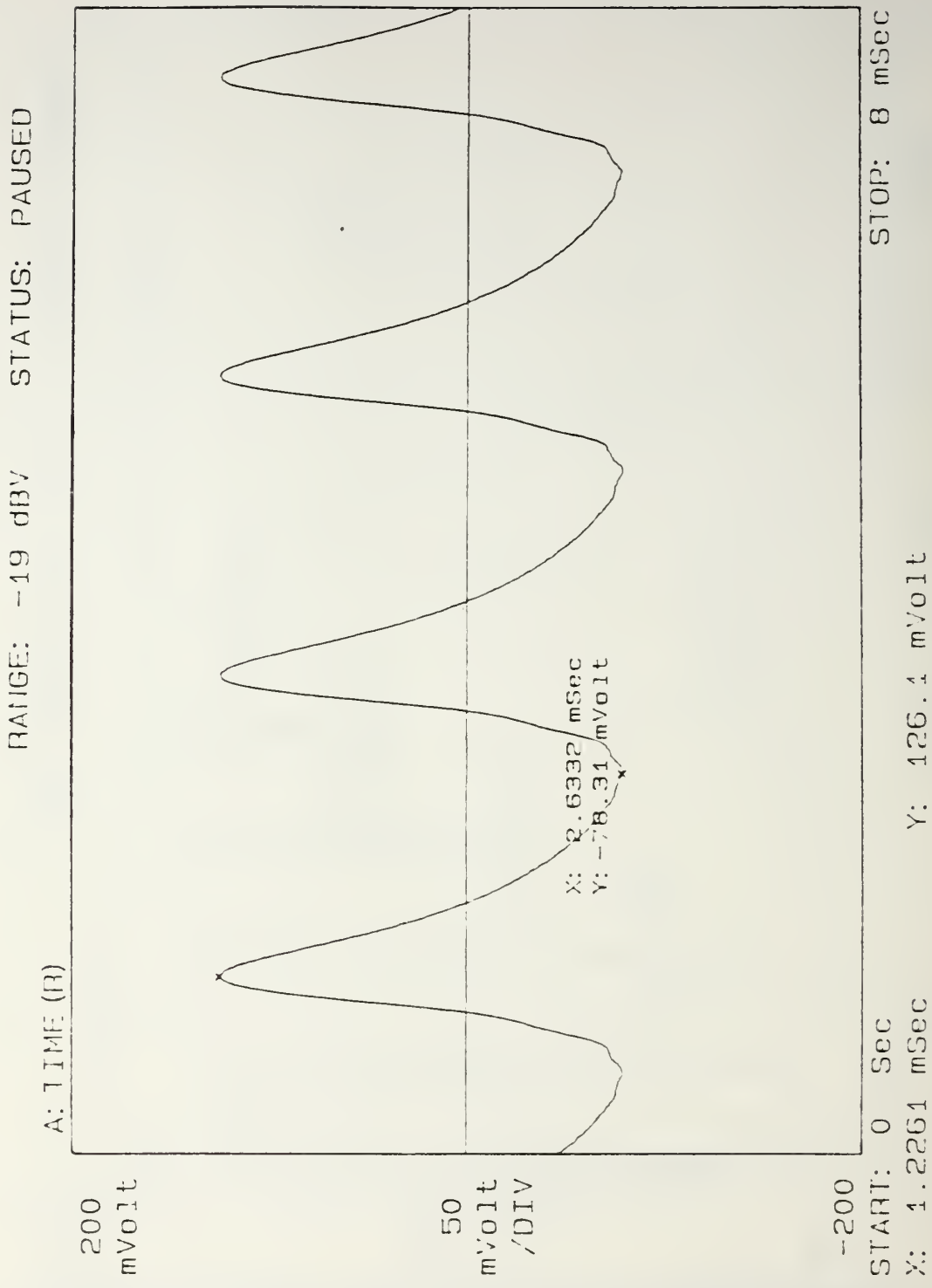

Figure 31 - Waveform of the sound generated by the prime mover at a temperature difference of 368 °C

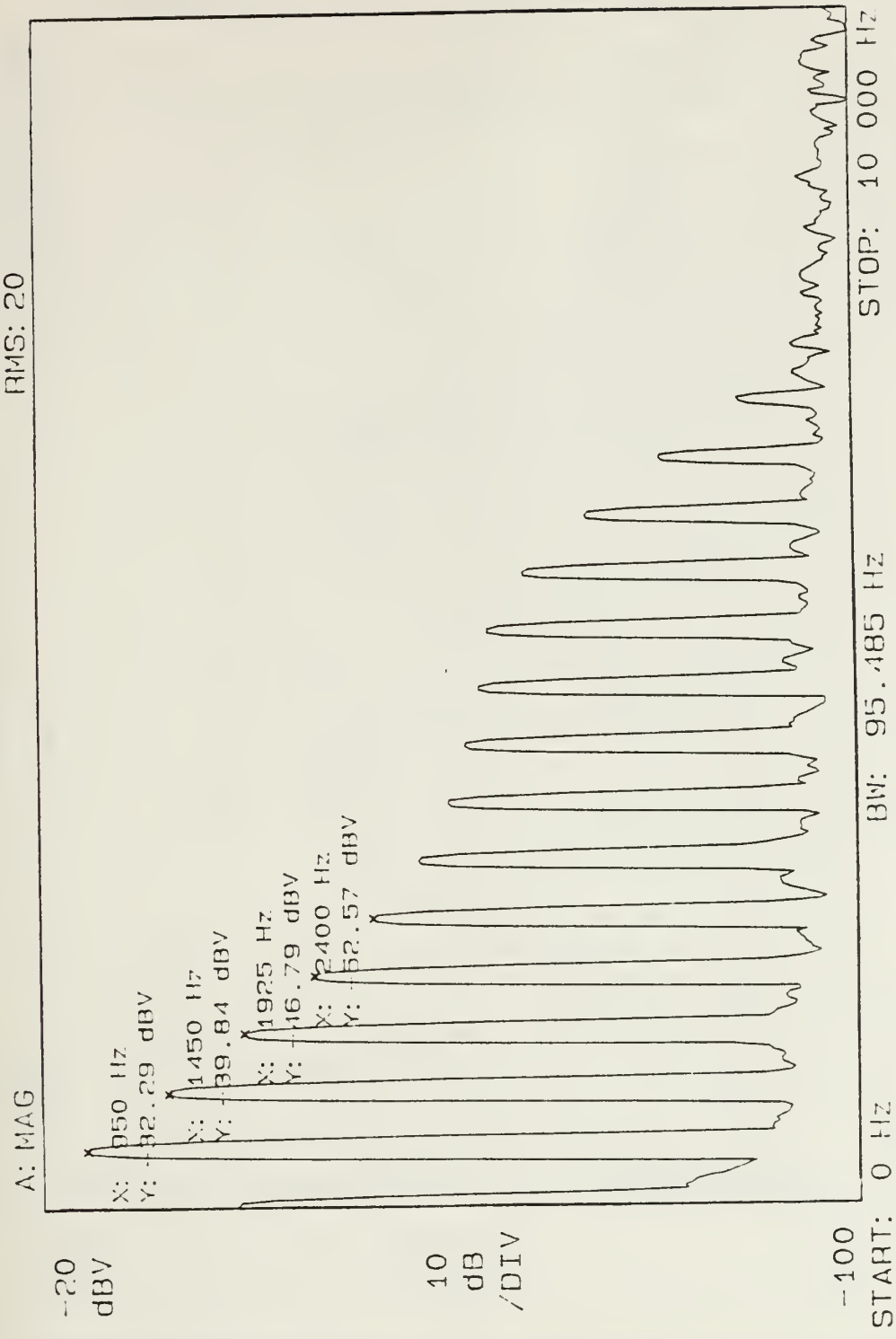

Figure 32 - Spectrum of the sound generated by the prime mover at a temperature difference of 368 °C

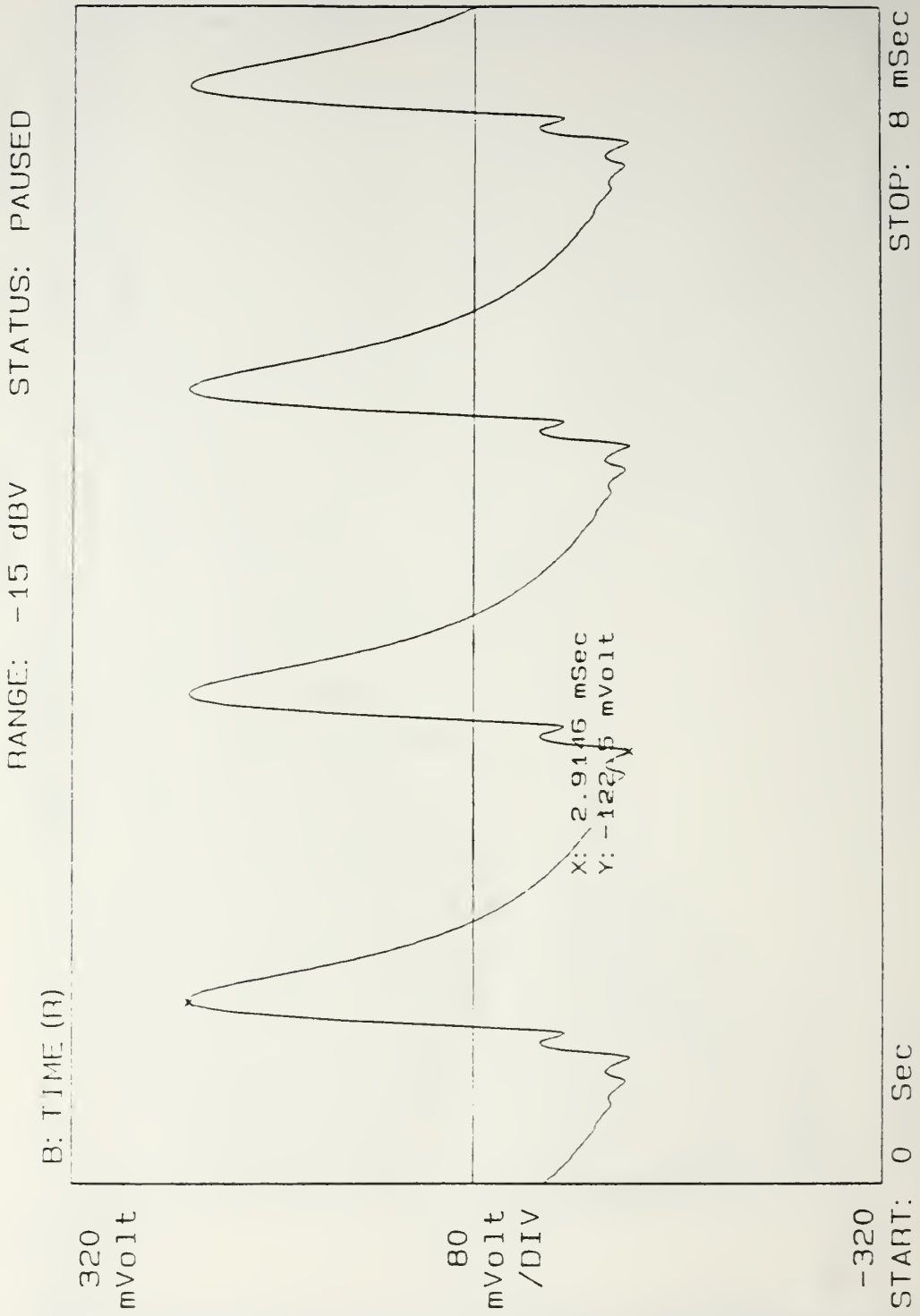

Figure 33 - Waveform of the sound generated by the prime mover at a temperature difference of 453 °C

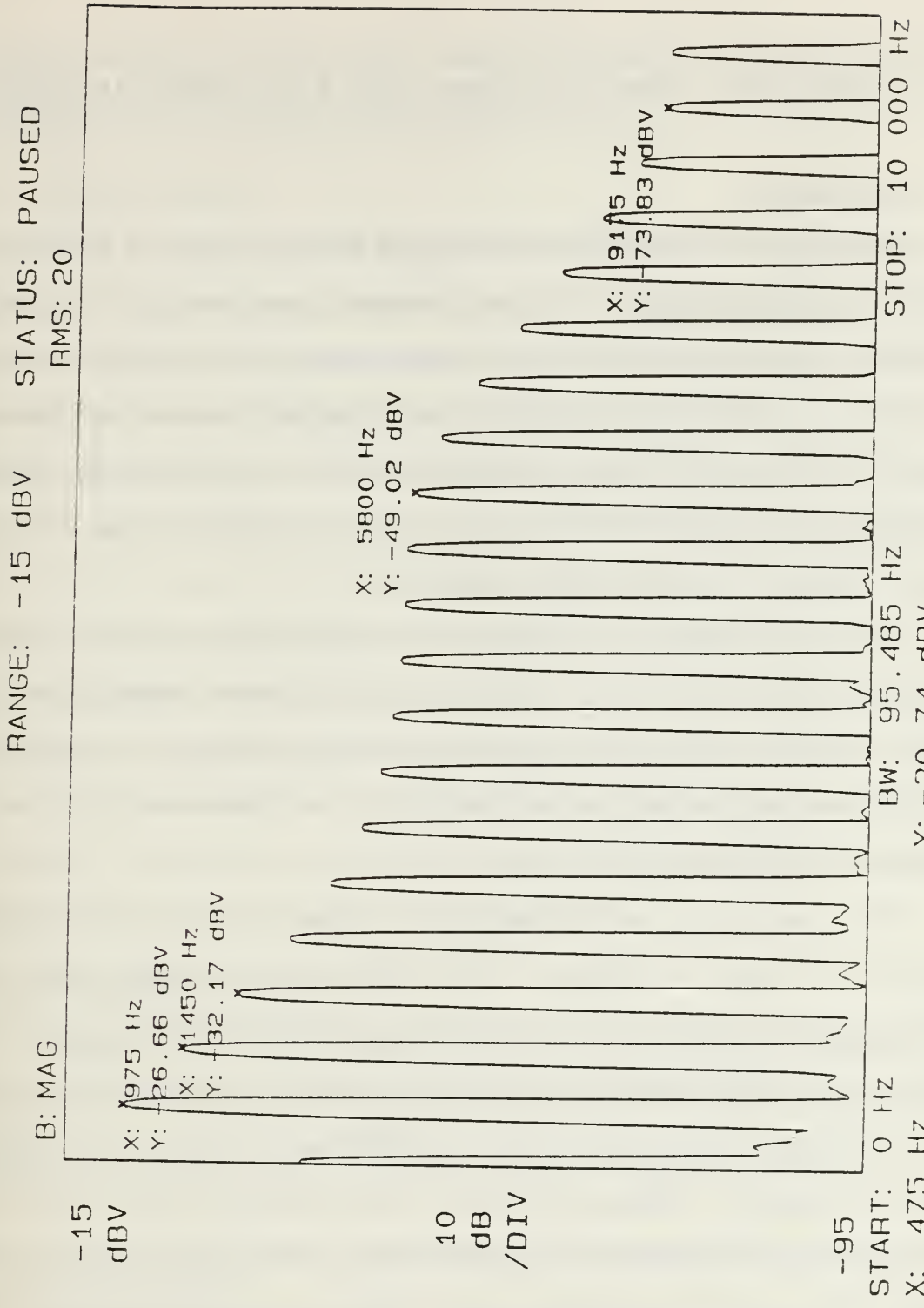

Figure 34 - Spectrum of the sound generated by the prime mover at a temperature difference of 453 °C

V. SUMMARY, CONCLUSIONS AND RECOMMENDATIONS

A. SUMMARY

The purpose of this thesis is to investigate the work output of a heat driven thermoacoustic prime mover. The experimental approach was to measure the frequency response of both a simple resonant tube and a prime mover for a variety of values for mean gas pressure and applied temperature difference across the prime mover stack. A least squares fit to a the frequency response yield the quality factor which can be compared to predictions based on a short stack, boundary layer approximation theory.

The results are reported of measurements made on the lowest three modes of the prime mover in helium for mean gas pressures between approximately 170 kPa to 500 kPa and the applied temperatures between zero and onset. The signal waveform of the sound generated by the prime mover above onset at a mean gas pressure of 307 kPa are also reported.

The overall results can be summarized as follows. Results of the resonant tube have at most 3% difference with theory. For the prime mover, the measurements generally agree with predictions for the fundamental mode except close to onset where the boundary layer approximation is not satisfied very well. This agreement between measured and predicted results worsens with decreasing mean gas pressure. Agreement is poor for the second and third modes for all pressures used, the source of the discrepancy may arise from the violation of the short stack assumption at higher modes. Finally, the sound generated by the

prime mover above onset has been noticeably distorted. The distortion becomes more severe as the temperature difference increases.

B. CONCLUSIONS

Several conclusions can be drawn from our results. The first conclusion is that the method used to determine the Q works well judging by the close agreement between theory and measurement for the simple resonant tube. The second conclusion is that short stack, boundary layer theory describes the fundamental mode of the prime mover below onset fairly well. There is generally good agreement with theory for low temperature differences, although the agreement worsens somewhat as onset is approached. The agreement also worsen as mean gas pressure decreases, probably due to the break down of the viscous boundary layer approximation. A third conclusion is that the short stack theory does not adequately describe higher modes, although the theory shows the same qualitative features as measurement. The final conclusion is that the sound generated by the prime mover above onset exhibits a great deal of nonlinear distortion. Reasons for this are not fully understood.

C. RECOMMENDATIONS

In order to gain better understanding of the thermoacoustic process and to determine the source of discrepancy, particularly for higher modes and the region close to onset, several recommendations are proposed as follows:

- Use a theory not limited by short stack and boundary layer approximations.
- Determine whether the nonlinear distortion seen above onset is primarily due to the presence of high amplitude waves in the resonator, independent of the presence of the stack, or if the stack is the dominant source of the distortion, or if both play equal roles.

APPENDIX A. PARTIAL LISTING OF THE PHYSICAL PROPERTIES OF HELIUM

TABLE 1: PHYSICAL PREPERTIES OF HELIUM [Ref. 6]

P	T	DEN	C_V	C_P	C	VISC	COND
MPA	K	KG/M^3	J/KG-K		M/S	PA-S*E+6	MW/M-K
0.170	293	0.280	3123	5197	1008	19.6	152.4
0.238	293	0.392	3123	5197	1008	19.6	152.4
0.308	293	0.504	3123	5197	1009	19.6	152.5
0.376	293	0.616	3123	5197	1009	19.6	152.5
0.507	293	0.833	3123	5197	1009	19.6	152.6

APPENDIX B. LISTING OF THE PHYSICAL PROPERTIES OF MATERIALS FOR THE PRIME MOVER STACK AND HEAT EXCHANGERS

TABLE 2: PHYSICAL PROPERTIES OF MATERIALS [Ref. 7-8]

MATERIAL	DEN$\left(\frac{KG}{M^3}\right)$	SPECIFIC HEAT$\left(\frac{J}{KG \cdot M}\right)$	COND$\left(\frac{W}{M \cdot K}\right)$
AISI 304 STAINLESS STEEL	8027	451.9	16.3
NICKEL	8890	443.8	89.9
COPPER	8900	384.0	350.0

APPENDIX C. LISTING OF THE SPECIFICATIONS OF THE COMPOMENTS AND GEOMETRICAL PARAMETERS OF THE PRIME MOVER

TABLE 3: SPECIFICATIONS OF THE COMPONENTS AND GEOMETRICAL PARAMETERS OF THE PRIME MOVER

•PRIME MOVER STACK			
Π= 205.8 cm	Δx = 3.50 cm	l = 0.0125 cm	y_o = 0.0395 cm
•HOT HEAT EXCHANGER			
Π = 148.3 cm	Δx = 0.762 cm	l = 0.0255 cm	y_o = 0.051 cm
•AMBIENT HEAT EXCHANGER			
Π= 83.7 cm	Δx = 2.032 cm	l = 0.0254 cm	y_o = 0.051 cm
•PARAMETERS OF PRIME MOVER			
x_{hot} = 0.950 m	x_{amb} = 0.883 m	$\bar{x}_{ex}^{hot}$ = 0.946 m	
$\bar{x}_{stack}$ = 0.925m	$\bar{x}_{ex}^{amb}$ = 0.894 m	R= 0.0191 m	
L = 1.0 m			

LIST OF REFERENCES

1. G. W. Swift, "Thermoacoustic engines," J. Acoust. Soc. Am. Vol. 84, 1145-1180 (1988).

2. John Wheatley, T. Hofler, G. W. Swift and A. Migliori, "Understanding some simple phenomena in thermoacoustics with applications to acoustical heat engines," Am. J. Phys. 53, 147-162 (1985).

3. John Wheatly, T. Hofler, G. W. Swift and A. Migliori, "An instrinsically irreversible thermoacoustic heat engine," J. Acoust. Soc. Am. Vol 74, 153-170 (1983).

4. John Wheatley, G. W. Swift and A. Migliori, "The Natural Heat Engine," Los Alamos Science, Fall 1986.

5. L. E. Kinsler, A. R. Frey, A. B. Coppens, and J. V. Sanders, "Fundamental of Acoustics," Third Edition, John Wiley & Sons, Inc., 1982.

6. McCarty R. D.,Thermodynamical Properties of Helium-4 from 2-1500 K with Pressure to 1000 Atmospheres, Washington D. C., NBS Technical Note 631, National Bureau of Standards, 1972.

7. Allegheny Ludlum Steel corporation, Stainless Steel Handbook, Allegheny Ludlum Steel Corporation, 1956.

8. Weast, Robert C., ed., CRC Handbook of Chemistry and Physics, 61st ed., Boca Raton, Flordia: CRC Press Inc., 1980.

INITIAL DISTRIBUTION LIST

	No. Copies
1. Library, Code 0142 Naval Postgraduate School Monterey, CA, 93943-5100	2
3. Prof. A. Atchley, Code 61Ay Department of Physics Naval Postgraduate School Monterey, CA, 93943	5
4. Dr. T. J. Hofler, Code 61Hf Department of Physics Naval Postgraduate School Monterey, CA, 93943	1
5. Dr. G. W. Swift Condensed Matter & Thermal Physics Los Alamos National Lab Los Alamos, NM, 87545	1
6. Dr. Henry E. Bass Department of Physics Naval Postgraduate School Monterey, CA, 93943	1
7. Prof. S. Baker, Code 61 Ba Department of Physics Naval Postgraduate School Monterey, CA, 93943	1
8. Prof. S. Garrett, Code 61Gx Department of Physics Naval Postgraduate School Monterey, CA, 93943	1

9. Library of Chung Cheng Institute of Technology — 1
Ta-Shih, Tao-Yuan, 33500
Taiwan, R. O. C.

10 Library of Chung San Institute of Science and Technology — 1
P.O. Box 1, Lung-Tan, Tao-Yuan, 33500
Taiwan, R. O. C.

11. Dr. Kuo, Shou-Shi — 1
Chairman of Department of Vehicle Engineering
Chung Cheng Institute of Technology
Ta-Shih, Tao-Yuan, 33500
Taiwan, R. O. C.

12. Lieutenant Richard Volkert — 1
Naval Underwater System Center
Newport, RI, 02841

13. Captain Michael Muzzerall — 1
301 Daniel Place
Victoria, British Columbia
Canada V9C 1W2

14. LCDR M. D. Kite — 1
709 Bruce Court
Herndon, VA, 22070

15. Ao, Chia-Ning — 1
25 Woon-Woo Rd.
Tai-Chung, 40403
Taiwan, R. O. C.

16. Captain Lin, Hsiao-Tseng — 4
Department of Vehicle Engineering
Chung Cheng Institute of Technology
Ta-Shih, Tao-Yuan, 33500
Taiwan, R. O. C.

17. LCDR Liu, Wei-Hsin — 1
SMC # 2636, Naval Postgraduate School
Monterey, CA, 93943

18. LCDR Chen, Chih-Lyeu 1
SMC # 1275, Naval Postgraduate School
Monterey, CA, 93943

19. Defense Technical Information Center 2
Cameron Station
Alexandria, VA, 22304-6145

411-387

GAYLORD S

AMERICAN BINDERY
TOPEKA KANSAS

thesL6433
Investigation of a heat driven thermoaco
3 2768 000 89051 1
DUDLEY KNOX LIBRARY